

# Amplification of cosmological inhomogeneities by the QCD transition

Christoph Schmid\*

*Institut für Theoretische Physik, ETH-Hönggerberg, 8093 Zürich, Switzerland*

Dominik J. Schwarz†

*Institut für Theoretische Physik, Universität Frankfurt, Postfach 11 19 32, 60054 Frankfurt am Main, Germany*

Peter Widerin‡

*Institut für Theoretische Physik, ETH-Hönggerberg, 8093 Zürich, Switzerland*

(Received 24 July 1998; published 28 January 1999)

The cosmological QCD transition affects primordial density perturbations. If the QCD transition is first order, the sound speed vanishes during the transition and density perturbations fall freely. For scales below the Hubble radius at the transition the primordial Harrison-Zel'dovich spectrum of density fluctuations develops large peaks and dips. These peaks grow with wave number for both the hadron-photon-lepton fluid and for cold dark matter. At the horizon scale the enhancement is small. This by itself does not lead to the formation of black holes at the QCD transition. The peaks in the hadron-photon-lepton fluid are wiped out during neutrino decoupling. For cold dark matter that is kinetically decoupled at the QCD transition (e.g., axions or primordial black holes) these peaks lead to the formation of CDM clumps of masses  $10^{-20}M_{\odot} < M_{\text{clump}} < 10^{-10}M_{\odot}$ . [S0556-2821(99)05702-1]

PACS number(s): 98.80.Cq, 12.38.Mh, 95.35.+d

## I. INTRODUCTION AND RESULTS

In the early universe a transition from a quark-gluon plasma (QGP) to a hadron gas (HG) took place at a certain transition temperature  $T_{\star}$ . At high temperatures the asymptotic freedom of QCD predicts the existence of a deconfined phase, the quark-gluon plasma. At low temperatures quarks and gluons are confined in hadrons. The deconfined phase at high temperatures was found by lattice QCD simulations [1]. The order of the QCD transition is still under debate, but recent lattice QCD results for three quark flavors with massive strange quarks indicate that the QCD transition is first order [2]. The value of the latent heat is available only for quenched lattice QCD (gluons only, no quarks) [3]. These data give a small latent heat  $l$ ; ( $l/T_{\star}$ ) is about one-fifth of the difference in entropies between an ideal massless quark-gluon plasma and hadron gas, respectively. Two-flavor calculations give  $T_{\star} \approx 140$  MeV [4]. Ongoing and future heavy ion experiments at the world's largest colliders [Super Proton Synchrotron (SPS), BNL Relativistic Heavy Ion Collider (RHIC), CERN Large Hadron Collider (LHC)] are searching for the QGP [5].

At the QCD transition the Hubble radius  $R_H \sim m_{\text{pl}}/T_{\star}^2$  is about 10 km. The mass inside a Hubble volume is  $\sim 1M_{\odot}$ . The transition lasts about a tenth of a Hubble time,  $t_H$ , with the latent heat from quenched lattice QCD. The Hubble time at the QCD transition is  $t_H = R_H/c \sim 10^{-5}$  s. This is extremely long in comparison with the relaxation time scale of the strong interactions, which is about  $10^{-23}$  s. Thus, the transition is very close to an equilibrium process.

For a first-order QCD transition hadronic bubbles nucleate during a short period of supercooling. The crucial parameters for supercooling are the surface tension  $\sigma$  and the latent heat  $l$ . Data for  $\sigma$  and  $l$  are available only for quenched QCD [3] and give a very small surface tension. This gives a very short period of supercooling,  $\Delta t_{\text{sc}} \sim 10^{-3}t_H$ , and a typical bubble nucleation distance  $d_{\text{nuc}} \approx 1 \text{ cm} \approx 10^{-6}R_H$  for homogeneous nucleation [6,7]. The hadronic bubbles grow very fast, within  $10^{-6}t_H$ , until the released latent heat has reheated the universe to  $T_{\star}$ . For the remaining 99% of the transition the HG and the QGP coexist at the pressure  $p_{\text{HG}}(T_{\star}) = p_{\text{QGP}}(T_{\star})$ . During this time the hadronic bubbles grow slowly and the released latent heat keeps the temperature constant until the transition is completed. The energy density decreases continuously from  $\rho_{\text{QGP}}(T_{\star})$  at the beginning of the transition to  $\rho_{\text{HG}}(T_{\star})$  when the transition is completed.

In the mid 1980s interest in the cosmological QCD transition arose because it was realized that a strongly first-order QCD phase transition with large surface tension could lead to observable signatures today. Witten [8] pointed out that the separation of phases during the coexistence of the hadronic and the quark phase could gather most baryons in (strange) quark nuggets. However, the quark nuggets, while cooling, lose baryons, and evaporize, unless they contain much more than  $10^{44}$  baryons initially [9]. This number should be compared with the number of baryons inside a Hubble volume at the QCD transition, which is  $10^{50}$ . Thus, the mean bubble nucleation distance should be  $> 10^{-2}R_H \sim 100$  m, which is about a factor  $10^4$  too big compared to the nucleation distance suggested using recent lattice results [3].

Applegate and Hogan found that a strongly first-order QCD phase transition with a large surface tension could induce inhomogeneous nucleosynthesis [10], assuming a nucleation distance which is ruled out by recent lattice re-

\*Email address: chschmid@itp.phys.ethz.ch

†Email address: dschwarz@th.physik.uni-frankfurt.de

‡Email address: widerin@itp.phys.ethz.ch

sults [3]. The large isothermal baryon fluctuations, induced during the separation of phases, could lead to inhomogeneous initial conditions for nucleosynthesis. As a minimal requirement for inhomogeneous nucleosynthesis the mean bubble nucleation distance should be larger than the proton diffusion length, which corresponds to  $\sim 3$  m [11] at the QCD transition. This is more than  $10^2$  times larger than the nucleation distance based on lattice results [3]. In addition, the observed cosmic abundances of light elements do not allow inhomogeneous nucleosynthesis, except in a small region in parameter space corresponding to an inhomogeneity scale of  $\sim 40$  m [11].

In a recent Letter [12] and in the present work we look at matter averaged over scales  $\lambda$  much larger than the bubble separation, e.g.  $\lambda$  of order of the Hubble radius  $R_H$ . Therefore we deal with the bulk properties of the fluid in contrast to previous investigations which dealt with physics at the bubble separation scale. We found that the evolution of cosmological density perturbations is strongly affected by a first-order QCD transition for subhorizon scales,  $\lambda < R_H$ . Preexisting cosmological perturbations with an approximate Harrison-Zel'dovich spectrum [13] are predicted by inflation [14–17] and have been observed in the temperature fluctuations of the cosmic microwave background by the COBE satellite [18].

We showed in [12] that pressure gradients and the isentropic sound speed (for wavelengths  $\lambda$  much larger than the bubble separation),  $c_s = (\partial p / \partial \rho)_S^{1/2}$ , must be zero during a first-order phase transition of a fluid with negligible chemical potential (i.e. no relevant conserved quantum number). The sound speed must be zero, because for such a fluid the pressure can only depend on the temperature,  $p(T)$ , and because the transition temperature  $T_*$  has a given value, it cannot depend on any parameter; hence  $p(T_*) = p_*$  is a given constant, and  $c_s = 0$ . This is in contrast e.g. to the water-vapor system, where the number of molecules is conserved, where the pressure also depends on the particle density in a given phase,  $p(T, n)$ , and where a two-phase system has an equilibrium pressure (the vapor pressure) which depends on the temperature,  $p_*(T)$ , and hence  $c_s \neq 0$ . During the entire QCD transition the sound speed stays zero and suddenly rises back to the radiation value  $c_s = 1/\sqrt{3}$  after the transition is completed. Pressure varies continuously and goes below the ideal radiation fluid value  $p = \rho/3$ , but stays positive. Jedamzik [19] independently pointed out that a significant decrease in the effective sound speed  $c_s$  during the cosmological QCD transition is expected.

Since the sound speed is zero during a first-order QCD transition, there are no pressure gradients and no restoring forces. Preexisting cosmological perturbations go into a free-fall. The superhorizon modes (at the time of the transition),  $\lambda > R_H$ , remain unaffected. The spectrum of subhorizon perturbations develops peaks in  $\delta\rho/\rho$  which grow with the wave number. The details of the enhancement depend on the QCD equation of state near  $T_*$ . The peaks grow at most linearly in wave number. The subhorizon peaks arise because preexisting acoustic oscillations at shorter wavelengths have a higher velocity (for a given  $\delta\rho/\rho$ ) at the beginning of the transition

and therefore get a larger amplification factor for  $\delta\rho/\rho$  during the transition.

Photons and relativistic leptons, i.e. the three neutrinos,  $e^\pm$  and  $\mu^\pm$ , also contribute to the energy density at the temperatures of interest. Weak and electro-magnetic interactions are fast enough to keep the photons and leptons in thermal equilibrium with the QGP-HG. Therefore the collective behavior of all these coupled particles can be described by one perfect (i.e. dissipationless) fluid, which we shall denote as radiation fluid (RAD).

As a second fluid we include cold dark matter (CDM) which dominates the energy density of the universe today. At the time of the QCD transition  $\rho^{\text{CDM}}(T_*) \sim 10^{-8} \rho^{\text{RAD}}(T_*)$ ; therefore the gravity generated by CDM can be neglected. We must distinguish two types of CDM with respect to the issue of kinetic decoupling at the time of the QCD transition. The lightest supersymmetric particle, which is probably the neutralino [20], is tightly coupled to the radiation fluid (and is treated as part of the RAD fluid) at  $T \sim T_*$ . The scattering rate of the neutralino is of the order of the weak interaction scattering rate; the neutralino decouples kinetically at a much lower temperature of a few MeV. Kinetic decoupling must be distinguished from freeze-out (when the pair production and annihilation rates fall below the Hubble rate), which happens way before the QCD transition. In contrast the second type of CDM is kinetically decoupled at the QCD transition, e.g. axions or preexisting primordial black holes. Note that in our figures and equations kinetically decoupled CDM will be labeled by CDM for brevity.

Kinetically decoupled CDM falls into the potential wells provided by the dominant radiation fluid. Thus, the CDM spectrum is amplified on subhorizon scales. The peaks in the CDM spectrum go nonlinear shortly after equality. This leads to the formation of CDM clumps with mass  $< 10^{-10} M_\odot$ . Especially the clumping of axions has important implications for the axion searches using the magnetic field induced axion decay [21].

The formation of primordial black holes (PBHs) should be particularly efficient during the QCD epoch due to a substantial reduction of pressure forces during adiabatic collapse as pointed out by Jedamzik [19]. The PBH mass function is expected to exhibit a pronounced peak on the QCD-horizon mass scale  $\sim 1 M_\odot$ . He proposes that these black holes could account for massive compact halo objects (MACHOs) observed by microlensing [22]. However, we found by our linear analysis [12] that the amplification of fluctuations at the QCD horizon crossing scale is only a factor 1.5. For standard models of structure formation without tilt, the amplitudes are not big enough to produce a cosmologically relevant amount of black holes [23]. A tilted spectrum could be fine-tuned to produce black holes at the QCD scale, but the spectrum would need a break just below the QCD scale in order not to overproduce smaller black holes. With the need of such a doubly fine-tuned preexisting spectrum the main effect would not be due to the QCD transition.

The influence of the QCD transition on primordial gravitational waves has been investigated by one of the present authors in Ref. [24]. It was found that the dramatic drop in relativistic degrees of freedom during the QCD transition

(from 51.25 in the QGP to 17.25 in the HG) induces a step by 30% in the primordial spectrum of gravitational waves. Today this step is located at  $\sim 10^{-8}$  Hz. Gravitational waves with that frequency could be detected by pulsar timing; however, for gravitational waves from inflation the amplitudes are far too small to show up in the pulsar timing residuals.

This paper is organized as follows: A discussion of hot QCD, bubble nucleation, and the vanishing of the sound speed for wavelengths  $\lambda$  much larger than the bubble separation can be found in Sec. II. In this section we present a fit to recent lattice QCD results. We give the thermodynamical curves for  $w=p/\rho$  and the sound speed  $c_s^2$  as a function of the scale factor at the QCD transition for three cases: the bag model [25], which gives a simple parametrization, our fit to lattice QCD and a smooth crossover.

In Sec. III we derive the amplification of density perturbations at the QCD transition both numerically and analytically. We present the evolution equations for cosmological perturbations in a first-order form in a uniform expansion gauge, which gives the same simple structure for the general relativistic dynamics as for the Jeans equations. The details of the amplification depend on the equation of state at the phase transition. We present three cases: First, we use the bag model [25], which allows a simple discussion of the effects. In the bag model, the amplification of subhorizon perturbations grows linearly in wave number  $k$ . Next, we use our fit to recent lattice QCD data [26,27], which indicate a smaller latent heat [3]. The amplifications for the lattice fit grow proportional to  $k^{3/4}$ . As a third example we study the possibility of a smooth crossover [28]. In this case, the sound speed stays finite and subhorizon scales are not amplified. The spectrum for a crossover has peaks only around the horizon scale. We prove that the spectra of primordial perturbations are not affected for scales greater than the Hubble horizon  $R_H$  at the transition.

In the last section (Sec. IV) we discuss observable consequences of the large peaks and dips in the spectrum of density fluctuations. Collisional damping around the time of neutrino decoupling wipes out all subhorizon inhomogeneities in the radiation fluid before big bang nucleosynthesis (BBN), and homogeneous BBN cannot be affected. We discuss black hole formation during the QCD transition and conclude that it is highly unlikely unless the primordial spectrum is fine-tuned at the QCD scale.

The most interesting prediction is the clumping of those types of CDM which are kinetically decoupled at the QCD transition and do not suffer from collisional damping by neutrinos. E.g. axions, if they are the CDM, are not distributed smoothly within the halo of our galaxy, they come in clumps.

Throughout the paper we assume that our universe is spatially flat ( $\Omega=1$ ) and most of its matter is CDM today. Whenever we give numbers we use a Hubble parameter of  $H_0=50 \text{ km s}^{-1} \text{ Mpc}^{-1}$ .

## II. COSMOLOGICAL QCD TRANSITION

### A. Hot QCD

The baryon number density in the universe is extremely small compared to the entropy density, i.e.  $n_B/s$

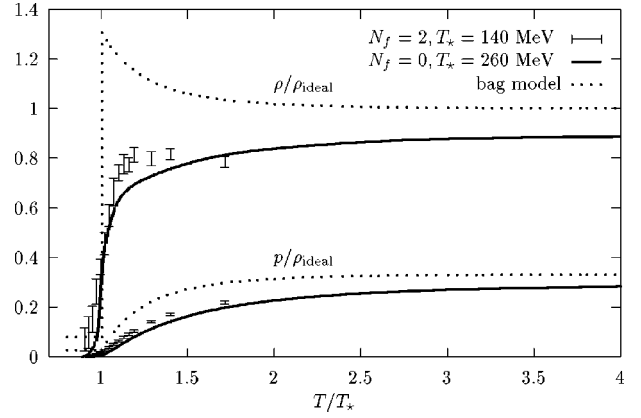


FIG. 1. The energy density and the pressure of hot QCD relative to the energy density of an ideal quark-gluon plasma are plotted as a function of  $T/T_*$ . The lattice QCD data for  $N_f=0$  [26] and  $N_f=2$  QCD [4] are compared with the predictions of the bag model.

$=\mathcal{O}(10^{-10})$ . At the time of the QCD transition the chemical potential for quarks and baryons, respectively, is negligible as far as the pressure  $p$  and energy density  $\rho$  are concerned,  $\rho$  and  $p$  depend on the temperature only.

The behavior of  $\rho(T)$  and  $p(T)$  near the QCD transition must be given by nonperturbative methods, lattice QCD. In Fig. 1 we plot lattice QCD data for  $\rho(T)$  and  $p(T)$  divided by  $\rho$  of the corresponding ideal gas. We show the lattice results for two systems, quenched QCD (no quarks) [26] and two-flavor QCD [27]. For quenched QCD the lattice continuum limit is shown. For two flavor QCD the data with six time steps ( $N_t=6$ ,  $a\approx 0.2 \text{ fm}$ ) and a quark mass  $am_q=0.0125$  are shown. This corresponds to a physical mass  $m_q\sim 14 \text{ MeV}$ , a bit heavier than the physical masses of the up and down quarks. On the horizontal axis we plot  $(T/T_*)$ . We note that the critical temperature for quenched QCD is  $T_*\sim 260 \text{ MeV}$  [26], and for two-flavor QCD  $T_*\sim 140 \text{ MeV}$  [4]. Unfortunately  $\rho(T)$  and  $p(T)$  for three quarks (u,d,s) with physical masses are not available yet. For  $T/T_*=4$  energy density and pressure for quenched QCD are still 10% and 15%, respectively, below the ideal gas value. It is remarkable that  $\rho/\rho_{\text{ideal}}$  and  $p/p_{\text{ideal}}$  versus  $T/T_*$  is quite similar for quenched QCD and two-flavor QCD. Moreover, the temperature dependence of the rescaled pressure for four-flavor QCD [29] is quite similar to quenched QCD.

At temperatures below  $T_*$  quarks and gluons are confined to hadrons, mostly pions. At present the hot pion phase is not seen in the two-flavor lattice QCD, since the pion comes out too heavy ( $0.3 < m_\pi/m_\rho < 0.7$  from [4], whereas the physical ratio is 0.18).

The second law of thermodynamics connects pressure and energy density, and reads, for a fluid without a chemical potential (no relevant conserved quantum numbers),

$$\rho = T \frac{dp}{dT} - p. \quad (2.1)$$

The Maxwell relation for the free energy gives the entropy density,

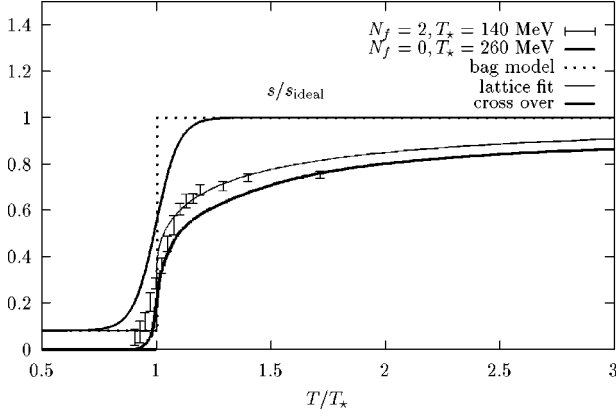


FIG. 2. The entropy density of hot QCD relative to the entropy density of an ideal QGP is shown for the same lattice QCD results as in Fig. 1. We also plot the entropy density for our fit to the lattice QCD data, for the bag model, and for a smooth crossover.

$$s = \frac{dp}{dT}. \quad (2.2)$$

From homogeneity the free energy density  $f(T) = -p(T)$ , and  $f(T)$  contains the full thermodynamic information. The lattice QCD results for  $s/s_{\text{QGP}}^{\text{ideal}}$  are shown in Fig. 2.

The bag model gives a simple parametrization for  $p(T)$  and hence for  $\rho(T), s(T)$ . The bag model ansatz represents the short-distance dynamics by an ideal gas of quarks and gluons and the long-distance confinement effects by a constant negative contribution to the pressure, the bag constant  $B$ ,

$$p_{\text{QGP}}(T) = p_{\text{QGP}}^{\text{ideal}}(T) - B. \quad (2.3a)$$

We include gluons and u,d quarks, which are effectively massless at  $T \approx T_*$ ; hence  $p_{\text{QGP}}^{\text{ideal}}(T) = (\pi^2/90)g_{\text{QGP}}^*T^4$ , where  $g^*$  is the effective number of relativistic helicity states,  $g^* = g_{\text{bosons}} + 7/8g_{\text{fermions}}$ ,  $g_{\text{QGP}}^* = 37$ . The low temperature phase is a hadron gas. We model it as an ideal gas of massless pions,

$$p_{\text{HG}} = \frac{\pi^2}{90}g_{\text{HG}}^*T^4, \quad (2.3b)$$

because the contribution of pions is small anyway,  $g_{\text{HG}}^*/g_{\text{QGP}}^* = 3/37$ .

At the phase transition ( $T = T_*$ ) the quark-gluon phase and the hadron phase have the same pressure,  $p = p_*$ . The stable phase for  $T \neq T_*$  is the one which gives the minimum for the free energy density  $f(T)$ , hence a maximum for  $p(T)$ . The condition for pressure equilibrium at  $T_*$  gives the relation between  $T_*$  and  $B$ ; using Eqs. (2.3a) and (2.3b) we obtain

$$B = \frac{\pi^2}{90}(g_{\text{QGP}}^* - g_{\text{HG}}^*)T_*^4. \quad (2.4)$$

We take  $T_*$  from lattice QCD calculations with two flavors, which give  $T_* \in (140, 160)$  MeV [1,4]. This corresponds to a

range of bag constants  $B^{1/4} \in (195, 221)$  MeV. This range is in agreement with fits to the light-hadron masses, which yield  $B^{1/4} = 145 - 245$  MeV (a compilation of various bag model light-hadron fits can be found in [30]). We adopt the value  $T_* = 150$  MeV.

Energy density and entropy density in the bag model follow from Eqs. (2.1)–(2.3a),

$$\rho_{\text{QGP}} = \rho_{\text{QGP}}^{\text{ideal}} + B \quad (2.5a)$$

$$s_{\text{QGP}} = s_{\text{QGP}}^{\text{ideal}}, \quad (2.5b)$$

with  $\rho^{\text{ideal}} = (\pi^2/30)g^*T^4$  and  $s^{\text{ideal}} = (2\pi^2/45)g^*T^3$  for massless particles. The bag results for  $\rho/\rho_{\text{QGP}}^{\text{ideal}}$ ,  $p/\rho_{\text{QGP}}^{\text{ideal}}$ ,  $s/s_{\text{QGP}}^{\text{ideal}}$  are shown in Fig. 1 and Fig. 2. Note that  $s/T^3$  is a simple step function in the bag model. The QCD transition is first order in the bag model, and the latent heat per unit volume,  $l \equiv T_*\Delta s$ , is

$$l = \frac{2\pi^2}{45}\Delta g^*T_*^4 = 4B, \quad (2.6)$$

where  $\Delta g \equiv g_{\text{QGP}} - g_{\text{HG}}$ .

The order of the QCD phase transition and (for a first-order transition) the magnitude of the latent heat is still a subject of debate. In quenched QCD the phase transition is of first order [26]. The latent heat was determined to be  $l \approx 1.4T_*^4$  [3]. It is useful to take the ratio  $R_L$  of the latent heat to the value  $T_*\Delta s^{\text{ideal}}$ , where  $\Delta s^{\text{ideal}}$  is the difference in entropy between an ideal massless HG and an ideal massless QGP,

$$R_L \equiv \frac{l}{(T_*\Delta s)^{\text{ideal}}} = \begin{cases} 1 & \text{bag model,} \\ 0.2 & \text{quenched lattice QCD.} \end{cases} \quad (2.7)$$

For two light quarks it is likely that the transition is a crossover [4,27]. This is in agreement with theoretical considerations [31], which predict a second-order phase transition in the massless quark limit. For three light flavors and for the physically relevant case of two light and one heavy flavor the phase transition is likely to be of first order [2]. This result was obtained using the Wilson quark action, whereas results with staggered quarks [32] indicate a crossover for the physical quark masses. For four quark flavors the transition is first order [29]. Since the latent heat for lattice QCD is known for quenched QCD only, we decided to use the latent heat ratio  $R_L = 0.2$  from quenched QCD as an indication for the physical case.

We also need an analytic representation of the lattice QCD data. We decided to fit the entropy density (Fig. 2) and to derive the other thermodynamic quantities with Eqs. (2.1) and (2.2). Below  $T_*$  we consider again an ideal gas of the three pions. We fit the shape of the lattice QCD data by

$$\frac{s^{\text{fit}}}{(2\pi^2/45)T^3} = g_{\text{HG}}^* + \Delta g^* \theta(T - T_*) \times \left[ R_L + (1 - R_L) \left( 1 - \frac{T_*}{T} \right)^\gamma \right]. \quad (2.8)$$

A good fit for our purpose is obtained for  $\gamma \in (0.3, 0.4)$ . We fix  $\gamma = 1/3$ . The fit is plotted in Fig. 2.

Finally, we do not neglect the possibility that the QCD transition could be a smooth crossover. Such a crossover has been modeled by a simple interpolation between the ideal values of the entropy density with a tanh. It was first given in Ref. [28] and is used in relativistic hydrodynamical simulations of heavy-ion collisions [33]. The entropy density is written as

$$\frac{s^{\text{crossover}}}{s_{\text{QGP}}^{\text{ideal}}} = 1 - \frac{1}{2} \frac{\Delta g^*}{g_{\text{QGP}}^*} \left[ 1 - \tanh\left(\frac{T - T_*}{\Delta T}\right) \right]. \quad (2.9)$$

We choose  $\Delta T/T_* = 0.1$ ; see Fig. 2. This gives the shape of the initial rise of the lattice data, but it necessarily fails to give the slow rise at higher temperatures from  $s/s_{\text{QGP}}^{\text{ideal}} \approx 0.6$  to 1. Comparing this model to the bag model and the lattice fit allows us to identify phenomena caused by the cosmological QCD transition that are independent of the order of the transition. The effects for wavelengths close to the Hubble scale will be shown to be approximately independent of the order of the transition.

The early universe at  $T$  around 150 MeV also contains photons and relativistic leptons ( $e^\pm, \mu^\pm$ , neutrinos) with a pressure

$$p_{1\gamma} = \frac{\pi^2}{90} g_{1\gamma}^* T^4, \quad (2.10)$$

where  $g_{1\gamma}^* = 14.25$ . We use the subscript minus to denote the value of some quantity at the beginning of the transition, i.e. when the universe has cooled to  $T_*$  from above, and the subscript plus to denote the value of the same quantity at the end of the transition, i.e. when the temperature starts to decrease again.

## B. Bubble nucleation

The expansion of the Universe is very slow compared to the strong, electro-magnetic, and weak interactions around  $T_*$ . To be more explicit, the rate of the weak interactions is  $\Gamma_w \sim G_F^2 T_*^5 \approx 10^{-14}$  GeV, the rate of the electro-magnetic interactions is  $\Gamma_{\text{em}} \sim \alpha^2 T_* \approx 10^{-5}$  GeV, and the rate of the strong interactions is  $\Gamma_s \sim \alpha_s^2(T_*) T_* \approx 10^{-1}$  GeV. These rates have to be compared to the Hubble rate  $H \sim T_*^2/m_{\text{Pl}} \approx 10^{-21}$  GeV. Thus, leptons, photons, and the QGP-HG are in thermal and chemical equilibrium at cosmological time scales. All components have the same temperature locally, i.e. smeared over scales  $\lambda \sim 10^{-7} R_H$ . At scales  $\lambda > 10^{-7} R_H$  strongly, weakly, and electro-magnetically interacting matter makes up a single perfect (i.e. dissipationless) radiation fluid.

In a first-order phase transition the QGP supercools until hadronic bubbles are formed at  $T_{\text{sc}} < T_*$  [8,34,35]. Without

“dirt” the bubbles nucleate due to thermal fluctuations (homogeneous nucleation). The probability to nucleate a bubble by a thermal fluctuation is proportional to  $\exp(\Delta S)$ , where  $\Delta S$  is the change in entropy by creating a bubble. The second law relates  $\Delta S$  to the minimal work done in this process, which is the change in the free energy because the volume and temperature are fixed [36]. The change in free energy of the system by creating a spherical bubble with radius  $R$  is

$$\Delta F = \frac{4\pi}{3} (p_{\text{QGP}} - p_{\text{HG}}) R^3 + 4\pi\sigma R^2, \quad (2.11)$$

where  $\sigma$  is the surface tension. Bubbles can grow if they are created with radii greater than the critical bubble radius  $R_{\text{crit}}$ . Smaller bubbles disappear again, because the free energy gained from the bulk of the bubble is more than compensated by the surface energy in the bubble wall.  $R_{\text{crit}}$  is determined from the maximum value of  $\Delta F(R)$ ,  $R_{\text{crit}}(T) = 2\sigma[p_{\text{HG}}(T) - p_{\text{QGP}}(T)]^{-1}$ . At  $T_*$  the critical bubble size diverges, and no bubble can be formed. Finally, the probability to form a hadronic bubble with critical radius per unit volume and unit time is given by

$$I(T) = I_0 \exp\left(-\frac{\Delta F_{\text{crit}}}{T}\right), \quad (2.12)$$

with  $\Delta F_{\text{crit}} = 16\pi\sigma^3/[3(p_{\text{HG}} - p_{\text{QGP}})^2]$ . For small supercooling  $\eta \equiv 1 - T/T_* \ll 1$  we may evaluate  $(p_{\text{HG}} - p_{\text{QGP}})(T)$  by using the second law of thermodynamics, i.e.  $p_{\text{HG}} - p_{\text{QGP}} \approx l\eta$ , and thus

$$\Delta F_{\text{crit}} \approx \frac{16\pi}{3} \frac{\sigma^3}{l^2 \eta^2}. \quad (2.13)$$

For dimensional reasons the prefactor  $I_0 \sim T_*^4$ . A more detailed calculation of  $I_0$  within the bag model has been provided in [37]. It was shown in Ref. [7] that the temperature dependence of the prefactor  $I_0$  can be neglected for the calculation of the supercooling temperature  $T_{\text{sc}}$  in the cosmological QCD transition. Furthermore a purely numerical prefactor to  $T_*^4$  would be irrelevant for our purposes as explained after Eq. (2.15). Therefore the probability to form a critical bubble per unit volume and unit time can be written as

$$I \approx T_*^4 \exp(-A/\eta^2), \quad (2.14)$$

with  $A \equiv 16\pi\sigma^3/(3l^2 T_*)$ .

The surface tension  $\sigma$  is a crucial parameter for  $T_{\text{sc}}$  and  $R_{\text{crit}}$ . The absence of surface excitations in hadronic spectra suggests that  $\sigma^{1/3} \ll B^{1/4}$  [30]. In lattice QCD rather small values are found. The authors of Ref. [3] find that  $\sigma \approx 0.015 T_*^3$  for quenched lattice QCD. There are no values for unquenched QCD available yet. However, an upper bound was obtained for the case of four-flavor lattice QCD in Ref. [38], i.e.,  $\sigma < 0.1 T_*^3$ . Using the results from quenched lattice QCD we find  $A = 2.9 \times 10^{-5}$ .

After the first bubbles have been nucleated, they grow most probably by weak deflagration [34,39,40,6]. The deflagration front (the bubble wall) moves with the velocity

$v_{\text{def}} \ll 1/\sqrt{3}$  [41]. The energy that is released from the bubbles is distributed into the surrounding QGP by a supersonic shock wave and by neutrino radiation. This reheats the QGP to  $T_*$  and prohibits further bubble formation. The shock front propagates with a speed slightly above the sound speed. The amplitude of the shock is very small [39]. Neutrinos have a mean free path of  $10^{-7}T_H$  at  $T_*$ . If they do most of the heat transport, it goes with  $v_{\text{heat}} = \mathcal{O}(c)$ . A detailed calculation of the supercooling temperature in the cosmological QCD transition was given in Refs. [35,6]. These calculations assume small supercooling. The suppression of bubble nucleation due to already existing bubbles is neglected.

The supercooling temperature fraction  $\eta_{\text{sc}}$  turns out to be about the same for the schematic case of one single bubble nucleated per Hubble volume per Hubble time,

$$\eta_{\text{sc}} \approx \left[ \frac{A}{4 \ln(T_*/H_*)} \right]^{1/2} \approx 4 \times 10^{-4}, \quad (2.15)$$

or the realistic case obtained below of one bubble nucleated per  $\text{cm}^3$  per  $10^{-6}$  of a Hubble time, which needs a supercooling 20% larger. This small increase of 20% in  $\eta_{\text{sc}}$  makes the bubble nucleation rate larger by a factor  $10^{24}$ .

The time needed for the supercooling is given by  $\Delta t_{\text{sc}}/t_H = \eta_{\text{sc}}/(3c_s^2) = \mathcal{O}(10^{-3})$ . The critical size of the bubbles created at the supercooling temperature is

$$R_{\text{crit}}(\eta_{\text{sc}}) \approx \frac{2\sigma}{l\eta_{\text{sc}}} \approx 30 \text{ fm}. \quad (2.16)$$

Bubbles present at a given time have been nucleated typically during the preceding time interval  $\Delta t_{\text{nucl}} \equiv I/(dI/dt) = \mathcal{O}(10^{-6})$ . Using the relation between time and supercooling  $\eta$ ,  $d\eta/dt = 3c_s^2/t_H$ , we find  $\Delta t_{\text{nucl}}/t_H = \eta^3/(6Ac_s^2)$ . During this time interval each bubble has distributed released latent heat over a distance  $\approx \Delta t_{\text{nucl}}v_{\text{heat}}$ . This distance has a weak dependence on the precise value of  $\eta_{\text{sc}}$ , but the bubble nucleation rate increases exceedingly strongly with  $\eta$  until one bubble per volume  $\sim (\Delta t_{\text{nucl}}v_{\text{heat}})^3$  is nucleated. Therefore the mean bubble separation is

$$d_{\text{nucl}} \approx v_{\text{heat}} \Delta t_{\text{nucl}} \approx \frac{v_{\text{heat}}}{3c_s^2} \frac{\eta_{\text{sc}}^3}{A} R_H = \mathcal{O}(10^{-6}R_H) = \mathcal{O}(1 \text{ cm}), \quad (2.17)$$

where we used  $v_{\text{heat}} = \mathcal{O}(c)$ ,  $c_s = \mathcal{O}(c)$ , which gives a typical value for the nucleation distance. In [7] the mean bubble nucleation distance due to thermal fluctuations (homogeneous nucleation) is calculated to be less than 2 cm, whereas for inhomogeneous nucleation (the first bubbles form at impurities like topological defects or primordial black holes) it might be a few m.

The above estimate of bubble separation applies if the limiting factor for quenching is the distribution of released latent heat by means of sound waves and by neutrino free streaming. On the other hand the limiting factor could be given by the rate of release of latent heat, i.e. by the bubble wall velocity  $v_{\text{def}}$ . Since the period of supercooling lasts about 1% of the time needed for completing the entire first-

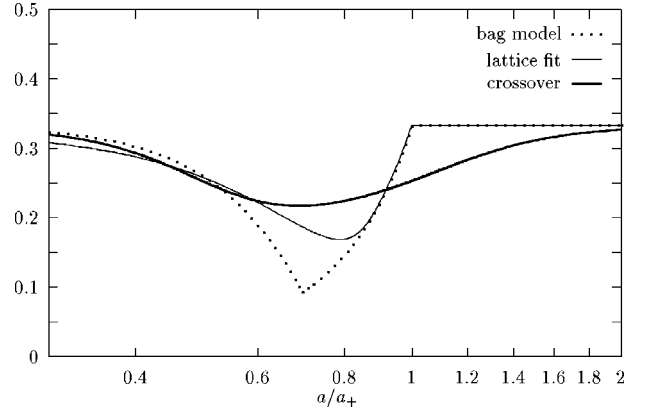


FIG. 3. The behavior of  $w = p/\rho$  during the QCD transition as a function of the scale factor  $a$ . Although the pressure is reduced, it stays positive throughout the transition.

order phase transition, 1% of the QGP must be converted to HG in the process of sudden reheating to  $T_*$ ; hence the bubble radius at quenching must reach 0.2 of the bubble separation,  $R_{\text{bubble}} \approx 0.2d_{\text{nucl}}$ . With  $R_{\text{bubble}} \approx v_{\text{def}}\Delta t_{\text{nucl}}$  and using the above relation  $d_{\text{nucl}} \approx v_{\text{heat}}\Delta t_{\text{nucl}}$ , we require  $v_{\text{def}} \geq 0.2v_{\text{heat}}$  for consistency. If  $v_{\text{def}}$  is smaller than this, the limiting factor for quenching is the rate of release of latent heat by bubble growth, and the bubble separation is

$$d_{\text{nucl}} \approx v_{\text{def}} \Delta t_{\text{nucl}} \approx \frac{v_{\text{def}}}{3c_s^2} \frac{\eta_{\text{sc}}^3}{A} R_H; \quad (2.18)$$

i.e., the bubble separation will be smaller than the estimate, Eq. (2.17).

To summarize, the scales on which non-equilibrium phenomena occur are given by the mean bubble separation, which is about  $10^{-6}R_H$ . The entropy production is tiny, i.e.  $\Delta S/S \sim 10^{-6}$ , since the supercooling is small  $\sim 10^{-3}$ . After supercooling, which lasts  $10^{-3}t_H$ , the universe reheats in  $\Delta t_{\text{nucl}} \approx 10^{-6}t_H$ . After reheating the thermodynamic variables follow their equilibrium values and bubbles grow due to the expansion of the Universe only. This is in striking contrast to bubble nucleation at the grand unified theory (GUT) transition, where the particle interaction rate is of the order of the Hubble rate and the bubble nucleation rate per unit volume is very much smaller than  $H^4$ .

### C. Adiabatic phase conversion

We now discuss the evolution of the temperature and other thermodynamic variables as a function of the scale factor  $a$ . The evolution of  $w \equiv p/\rho$  for the bag model, our lattice QCD fit, and for the smooth crossover (2.9) is shown in Fig. 3.

Entropy is conserved, apart from the very short stage of reheating ( $\sim 10^{-6}t_H$ ) after the first bubbles have been nucleated. This allows us to calculate  $T = T(a)$  from  $d[s(T)a^3] = 0$ , i.e.

$$\frac{dT}{d \ln a} = - \frac{3s}{ds/dT}, \quad (2.19)$$

except for  $T=T_*$  in the case of a first-order phase transition. In the bag model  $s \sim T^3$  and therefore  $T \propto 1/a$  for  $T \neq T_*$ . In the case of the lattice fit and the crossover the entropy is given by Eq. (2.8) and Eq. (2.9), respectively, plus the contribution of photons and leptons. Pressure as a function of the scale factor is obtained from  $s = dp/dT$ , using Eq. (2.19). The energy density, hence  $w$ , follows from Eq. (2.1).

While the QGP and HG coexist in a first-order QCD transition, the expansion factor is determined by entropy conservation,

$$\frac{a_+}{a_-} = \left( \frac{s_-}{s_+} \right)^{1/3}, \quad (2.20)$$

where the index  $-$  ( $+$ ) denotes the value of a quantity at the beginning (end) of the coexistence epoch. In the bag model the Universe expands by a factor  $a_+/a_- \approx 1.4$  until all QGP has been converted into the HG, whereas for our lattice QCD fit (2.8) the Universe expands by a factor  $a_+/a_- \approx 1.1$ . The growth of the scale factor is related to a lapse in cosmic time by  $d \ln a = H dt$ . In terms of Hubble time the transition lasts  $0.3 t_H$  for the bag model and  $0.1 t_H$  for our lattice QCD fit.

During a first-order QCD transition, i.e.  $T=T_*$ , the pressure  $p(T_*) \equiv p_*$  is constant. For any first-order QCD phase transition  $\rho(a)$  is obtained from the first law of thermodynamics  $d\rho = -3(\rho + p_*) da/a$ . The result for  $a_- \leq a \leq a_+$  is

$$\rho(a) = (\rho(a_-) + p_*) \left( \frac{a_-}{a} \right)^3 - p_*, \quad (2.21)$$

$$w(a) = \left[ \left( \frac{\rho(a_-)}{p_*} + 1 \right) \left( \frac{a_-}{a} \right)^3 - 1 \right]^{-1}, \quad (2.22)$$

where  $w \equiv p/\rho$ . After the end of the phase transition we have made the approximation of noninteracting and massless pions, leptons and photons,  $p = \rho/3$ , and therefore  $p_* = \rho(a_+)/3$ .

#### D. Sound speed

As explained in the Introduction, the isentropic sound speed (for wavelengths  $\lambda$  much larger than the bubble separation), given by

$$c_s^2 = \left( \frac{\partial p}{\partial \rho} \right)_s = \left( \frac{dp/da}{d\rho/da} \right)_s, \quad (2.23)$$

must be zero during a first-order phase transition for a fluid with negligible chemical potential (i.e. no relevant conserved quantum number). This behavior is shown in Fig. 4 for the lattice QCD fit and the bag model. In the bag model  $c_s^2 = 1/3$  before and after the transition. For a crossover the sound speed does not drop to zero.

A strong decrease in the sound speed is observed in lattice QCD for  $N_f=0$  [26] and for  $N_f=2$  [4]. From our lattice QCD fit we can calculate the sound speed for  $T > T_*$ . From Eq. (2.1) and Eq. (2.2) the sound speed is given by  $c_s^2 = (d \ln s / d \ln T)^{-1}$ . Inserting Eq. (2.8), we obtain

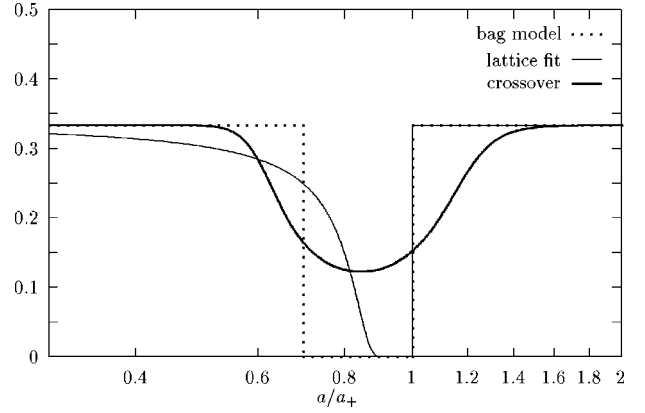


FIG. 4. The behavior of the sound speed  $c_s^2 = (\partial p / \partial \rho)_s$  during the QCD transition as a function of  $a$ . For a first-order transition (lattice fit and bag model) the sound speed vanishes.

$$c_s^2 \propto \left( 1 - \frac{T_*}{T} \right)^{1-\gamma}. \quad (2.24)$$

For an analytic discussion of the behavior of acoustic modes during the phase transition it is important to know  $c_s^2$  as a function of conformal time  $\eta \equiv \int a^{-1}(t) dt$ . In the radiation dominated regime  $a \propto \eta$ . Up to small corrections, this holds true during the transition. Let us denote the value of conformal time at which the sound speed vanishes by  $\eta_-$ . From Eq. (2.19) we find  $(\eta_- - \eta) / \eta_- \propto (1 - T_*/T)^\gamma$ , which implies

$$c_s^2 = C^2 [(\eta_- - \eta) / \eta_-]^{(1-\gamma)/\gamma}, \quad (2.25)$$

with  $C^2 = \{3^{1-\gamma} [g_+^* + \Delta g^* R_L] / [\Delta g^* (1 - R_L)]\}^{1/\gamma}$ . For  $\gamma = 1/3$  the sound speed goes to zero linearly in conformal time.

We now discuss why the isentropic condition applies during the part of the phase transition after the initial supercooling, bubble nucleation, and sudden reheating to  $T_*$ . During the second part of the transition, which takes about 99% of the transition time, the fluid is extremely close to thermal equilibrium, because the time to reach equilibrium is very much shorter than a Hubble time; i.e., the fluid makes a reversible transformation. This can be seen as follows. Across the bubble walls local pressure equilibrium is established immediately,  $p_{\text{QGP}} = p_{\text{HG}}$  locally. Local temperature equilibrium  $T_{\text{QGP}} = T_{\text{HG}}$  is established by neutrinos, which have a mean free path of  $10^{-7} R_H$ , enormously larger than the bubble wall thickness, and a collision time much shorter than the Hubble time. This local pressure and temperature equilibrium can only be satisfied if  $p = p_*$  and  $T = T_*$  at the bubble walls. Over distance scales of the order of the bubble separation ( $\sim 1$  cm) pressure (and therefore also temperature) is equalized with the velocity of sound, and thereby the released latent heat is distributed. This pressure equalization is very fast compared to the Hubble expansion velocity  $v_H \approx 10^{-6} c$  at the 1 cm scale. When analyzing cosmological perturbations we shall consider wavelengths  $\lambda > 10^{-4} R_H$ , for which neutrinos are tightly coupled,  $\Gamma_\nu / k \gg 1$ ; see Sec. IV. For these wavelengths the radiation fluid behaves as a

perfect (i.e. dissipationless) fluid, entropy in a comoving volume is conserved, and one has a reversible process. On the other hand, below the neutrino diffusion scale,  $\lambda < 10^{-4} R_H$ , acoustic oscillations are damped away before the QCD transition.

We have been criticized in [42] for the use of the isentropic condition. In [42] it was claimed that the isentropic condition leads to an infinite sound speed in the bag model. This claim was wrong, because it was based on non-relativistic hydrodynamical equations which neglect the pressure contribution to the momentum density and neglect that sound waves in a radiation fluid move with relativistic speed. In a revised version of their work [43] they correct these mistakes. However, they still maintain that the isentropic condition does not hold, but that instead the volume fraction of the two phases is frozen. They do not give any argument why such a freezing should occur, and their freezing assumption contradicts the rapid equilibration of pressure and temperature between the two phases explained in the previous paragraph. Their freezing assumption would also entail supercooling from the Hubble expansion in the presence of a finite volume fraction of bubbles. This is in dramatic conflict with the extremely rapid reheating to  $T_*$  (within  $10^{-6} t_H$ ) once enough bubbles ( $\sim 1\%$  of volume) have been formed as discussed in Sec. II B.

### III. PEAKS AND DIPS IN THE DENSITY SPECTRUM

#### A. Evolution equations for cosmological perturbations in uniform expansion gauge

The evolution of cosmological perturbations at the QCD transition is analyzed for perfect fluids. We linearize the Einstein equations, e.g.  $\rho(\mathbf{x}, t) = \rho_0(t) + \delta\rho(\mathbf{x}, t)$ . It is an excellent approximation at early times to take the Friedmann-Robertson-Walker metric flat,  $ds^2 = -dt^2 + a(t)^2 d\mathbf{x} \cdot d\mathbf{x}$ . The evolution of the background quantities is given by the Friedmann equations

$$H^2 = \frac{8\pi G}{3} \rho_0$$

$$\dot{H} = -4\pi G(\rho_0 + p_0), \quad (3.1)$$

where the subscript 0 denotes background quantities.

The perturbed metric is decomposed in a scalar, a vector, and a tensor part. We are only interested in density perturbations, which means the scalar (longitudinal) sector. For a time-orthogonal foliation of space-time the perturbed metric can be written as

$$ds^2 = -(1 + 2\alpha)dt^2 + a(t)^2[\delta_{ij}(1 + 2\varphi) + 2\partial_i\partial_j\gamma]dx^i dx^j, \quad (3.2)$$

with  $\partial_i \equiv \partial/\partial x^i$ . We follow Bardeen (1989) [16] and focus on the geometric properties of the constant- $t$  hypersurfaces (slices)  $\Sigma$ . The perturbation of the lapse function between the  $\Sigma$ 's is given by  $\alpha(\mathbf{x}, t)$ . The intrinsic curvature of  $\Sigma$  is generated by  $\varphi(\mathbf{x}, t)$ ,

$${}^{(3)}R[\Sigma] = -4\Delta\varphi. \quad (3.3)$$

The extrinsic curvature  $K^i_j$  of  $\Sigma$  has 3 terms, the unperturbed term, the perturbation of the isotropic part,  $\delta[\text{tr} K^i_j(\Sigma)] \equiv \kappa$ , and the anisotropic part ( $\equiv$  shear of normals on  $\Sigma$ ), which is generated by  $\chi(\mathbf{x}, t)$ ,

$$K^i_j[\Sigma] = -H\delta^i_j + \frac{1}{3}\kappa\delta^i_j - \left(\partial^i\partial_j - \frac{1}{3}\Delta\delta^i_j\right)\chi, \quad (3.4)$$

where  $\partial^i = a^{-2}\delta^{ij}\partial_j$ . These geometric properties of  $\Sigma$  are computed from the metric perturbations as follows:  $\chi = a^2\dot{\gamma}$ ,  $\kappa = -3(\dot{\varphi} - H\alpha) - \Delta\chi$ . Vanishing shear of  $\underline{n}(\Sigma)$  means  $\chi = 0$  and vice versa, but note that  $\chi$  (respectively,  $\gamma$ ) contributes both to the anisotropic part and to the isotropic part of  $K^i_j$ .

We choose a slicing of space-time with unperturbed mean extrinsic curvature,  $\delta[\text{tr} K^i_j(\Sigma)] \equiv \kappa = 0$ . This implies that our fundamental observers, which are defined to be at rest on the slice  $\Sigma$ ,  $\underline{u}(\text{obs}) = \underline{n}(\Sigma)$ , have relative velocities, which in the mean over all directions follow an unperturbed Hubble flow. If the coordinate choice (gauge choice) is such that the time coordinate  $t$  is constant on the slices  $\Sigma$ , the gauge is fixed to be the uniform expansion gauge (UEG)  $\equiv$  uniform Hubble gauge (UHG) [16].

In the literature the most common gauges are the synchronous gauge, where the fundamental observers are moving inertially (i.e.  $\alpha \equiv 0$ ), the longitudinal gauge ( $\equiv$  zero shear gauge,  $\chi \equiv 0$ ), where the fundamental observers expand isotropically, and the comoving gauge, where the fundamental observers sit in the fluid rest frame,  $\underline{u}(\text{obs}) = \underline{u}(\text{matter})$ . The uniform expansion gauge (UEG) is free of spurious gauge modes (in contrast to the synchronous gauge), it is nonsingular in the superhorizon limit and therefore easy to handle in numerical calculations (in contrast to zero-shear variables, as pointed out by Bardeen [16]), and it has the two basic fluid variables  $\delta\rho$  and  $v_{\text{peculiar}}$  (in contrast to the comoving gauge).

As fundamental evolution equations in UEG for perfect fluids we take the energy-momentum conservation  $\nabla_\mu T^\mu_\nu = 0$ , i.e., the continuity equation and (in the longitudinal sector) the 3-divergence of the Euler equation of general relativity. Each fluid separately must satisfy

$$\partial_t \epsilon = -3H(\epsilon + \pi) - \Delta\psi - 3H(\rho_0 + p_0)\alpha \quad (3.5)$$

$$\partial_t \psi = -3H\psi - \pi - (\rho_0 + p_0)\alpha, \quad (3.6)$$

where  $\epsilon \equiv \delta\rho = \delta T^0_0$ ,  $\pi \equiv \delta p = 1/3\delta[\text{tr} T^i_j]$ ,  $\nabla_i \psi \equiv \delta T^0_i$  for each fluid separately. Note that  $\nabla_i \psi \equiv S_i =$  momentum density (Poynting vector). The system of dynamical equations is closed by Einstein's  $R^0_0$ -equation

$$(\Delta + 3\dot{H})\alpha = 4\pi G(\epsilon + 3\pi), \quad (3.7)$$

where the sum over all fluids is taken on the right-hand side. In addition we need  $(p/\rho)$  and  $(\pi/\epsilon)_s = c_s^2$  (Figs. 3 and 4) for adiabatic perturbations. Equations (3.5)–(3.7) define our general relativistic Cauchy problem (linear perturbations, longitudinal sector, perfect fluids). The initial data  $(\epsilon, \psi)$  can be chosen freely on  $\Sigma_{\text{UE}}$ .

Einstein's  $R^0_0$ -equation in linear perturbation theory in the UEG is an elliptic equation. Its Green function is a Yukawa potential with exponential cutoff at the Hubble radius,  $\alpha \sim r^{-1} \exp(-\mu r)$ , where  $\mu^2 = -3\dot{H}$ , instead of Newton's  $1/r$ -potential in the Jeans equations.  $R^0_0$  gives the relative gravitational acceleration (geodesic deviation), averaged over all directions, of two test particles, which are moving nonrelativistically in the coordinate system at hand. In the UEG  $\delta R^0_0$  is determined by  $\alpha$ , the perturbation of the lapse. In Newtonian physics the relative acceleration averaged over directions is given by  $\Delta \Phi_{\text{Newton}}$ ; i.e.,  $R^0_0$  and  $\Delta \Phi_{\text{Newton}}$  answer the same physics question. In the UEG  $\alpha$  plays the role of the gravitational potential.

Our basic equations have exactly the same structure as the Jeans equations: two first-order time-evolution equations for each fluid, Eqs. (3.5) and (3.6), supplemented by one elliptic equation, Eq. (3.7). The UEG is the only gauge with this structure and with Einstein's equation appearing only in the elliptic equation. In the subhorizon limit [drop the last term in (3.5) and the  $\dot{H}$ -term in (3.7)] and with  $p \ll \rho$  these equations automatically reduce to the Jeans equations. The UEG is singled out for two reasons: First, the relative velocity of the fundamental observers in the mean over all directions is an unperturbed Hubble flow both in the UEG of general relativity and in the Jeans analysis. Second, only the mean over all directions appears in the continuity equation, in the 3-divergence of the Euler equation, and in the  $R^0_0$ -equation.

Out of the geometric quantities  $(\kappa, \chi, \varphi, \alpha)$  only the lapse  $\alpha$  appears in the equations needed to solve the dynamics in UEG. The spatial curvature ( $\varphi$ ) and the shear of the fundamental observers ( $\chi$ ) are automatically absent from the above equations for perfect fluids, since these geometrical properties of  $\Sigma$  are irrelevant for the dynamical question at hand.  $(\varphi, \chi)$  are not needed at all to solve the dynamics. One can compute  $\varphi$  and  $\chi$  at any time from the energy and the momentum constraints, i.e. from the  $G^0_0$  equation and the longitudinal contribution to the  $G^0_i$  equation,

$$\Delta \varphi = -4 \pi G \epsilon \quad (3.8)$$

$$\Delta \chi = -12 \pi G \psi. \quad (3.9)$$

This sequence, solving the dynamics before using the  $G^0_0$  and  $G^0_i$  constraint equations, is different from the usual solution strategies in linear perturbation theory.

Since the evolution equations are linear, and the background is spatially homogeneous, each spatial Fourier mode with comoving wavelength  $k := k^{\text{phys}} a$  evolves independently. It is convenient to rewrite Eqs. (3.5)–(3.7) in the dimensionless variables  $\delta \equiv \epsilon/\rho$  (density contrast),  $\hat{\psi} \equiv k_{\text{phys}} \psi/\rho$ . The variable  $\hat{\psi}$  is related to the fluid velocity (peculiar velocity)  $v_{\text{pec}} = [\rho/(\rho+p)] |\hat{\psi}|$  and has the same order of magnitude as  $\delta$  on subhorizon scales,  $\lambda^{\text{phys}} \ll R_{\text{H}} = H^{-1}$ . In the UEG the system of evolution equations, written in terms of conformal time  $(\ )' \equiv \partial_\eta \equiv a \partial_t$ , now reads

$$\frac{1}{\mathcal{H}} \delta' + 3(c_s^2 - w) \delta = \frac{k}{\mathcal{H}} \hat{\psi} - 3(1+w) \alpha \quad (3.10)$$

$$\frac{1}{\mathcal{H}} \hat{\psi}' + (1-3w) \hat{\psi} = -c_s^2 \frac{k}{\mathcal{H}} \delta - (1+w) \frac{k}{\mathcal{H}} \alpha \quad (3.11)$$

$$\left[ \left( \frac{k}{\mathcal{H}} \right)^2 + \frac{9}{2} (1+w) \right] \alpha = -\frac{3}{2} (1+3c_s^2) \delta, \quad (3.12)$$

with  $\mathcal{H} \equiv (da/d\eta)/a$  and  $w = p/\rho$ . The Friedmann equation and the continuity equation for the background were used. The continuity and Euler equations refer to each fluid separately. In the  $R^0_0$ -equation  $w = (\sum_f p^{(f)})/(\sum_f \rho^{(f)})$ ,  $\delta = (\sum_f \epsilon^{(f)})/(\sum_f \rho^{(f)})$  and  $c_s^2 = (\sum_f p^{(f)})/(\sum_f \epsilon^{(f)})$ .

In our numerical analysis we have used the exact general relativistic equations (3.10)–(3.12), but it is instructive to look at the superhorizon  $\lambda^{\text{phys}} \gg H^{-1}$  and at the subhorizon  $\lambda^{\text{phys}} \ll H^{-1}$  limit of Eqs. (3.10)–(3.12) for general pressure and sound speed.

For superhorizon perturbations with arbitrary equation of state (e.g. QCD transition), we only have to keep the lowest order in  $k/\mathcal{H}$  in the evolution equations. Equations (3.10)–(3.12) for a one fluid model simplify to

$$\frac{1}{\mathcal{H}} \delta' - (1+3w) \delta = \frac{k}{\mathcal{H}} \hat{\psi} \quad (3.13)$$

$$\frac{1}{\mathcal{H}} \hat{\psi}' + (1-3w) \hat{\psi} = \frac{1}{3} \frac{k}{\mathcal{H}} \delta, \quad (3.14)$$

where the superhorizon limit of the Poisson equation  $(1+w)\alpha = -\frac{1}{3}(1+3c_s^2)\delta$  was inserted. Note that the sound speed drops out in the superhorizon equations. For the growing mode the terms on the left hand side of the Euler equation add and  $[\hat{\psi}/\delta]_{\text{grow}} \propto k/\mathcal{H}$ . Therefore, the right hand side of the continuity equation is negligible and the solution for the growing mode of the density contrast is

$$\delta \propto (k/\mathcal{H})^2 = (k_{\text{phys}}/H)^2 \quad (3.15)$$

for superhorizon perturbations in the uniform expansion gauge. This result is independent of the thermodynamic behavior. It says that the evolution of the growing superhorizon mode, if expressed in terms of  $\mathcal{H}$  (as opposed to expressing it in terms of  $t$  or  $a$ ), is unaffected by a phase transition. Therefore the QCD-transition cannot affect superhorizon scales, and the spectrum of density perturbations stays flat for  $\lambda^{\text{phys}} \gg H^{-1}$ . This result can also be formulated differently: using the energy-constraint (3.8) we find  $\varphi = \text{const}$  for the dominant mode on superhorizon scales in the UEG. This is the ‘‘conservation law’’ [15] for the quantity  $\zeta \equiv \varphi + [1/3(1+w)]\delta$  for  $w \neq -1$ , since  $\zeta \approx \varphi$  in the superhorizon limit.

For subhorizon analysis,  $\lambda^{\text{phys}} \ll H^{-1}$ , with arbitrary equation of state, we can drop  $\dot{H}$  in the general relativistic Poisson equation (3.7) since  $|\dot{H}| = O(H^2) \ll k_{\text{phys}}^2$ . In the continuity equation (3.5) the time dilation term (last term) can be omitted since it follows from the Poisson equation that  $\alpha = O(H^2/k_{\text{phys}}^2) \delta \ll \delta$ . In the subhorizon limit Eqs. (3.10)–(3.12) simplify to

$$\frac{1}{\mathcal{H}}\delta' + 3(c_s^2 - w)\delta = \frac{k}{\mathcal{H}}\hat{\psi} \quad (3.16)$$

$$\frac{1}{\mathcal{H}}\hat{\psi}' + (1 - 3w)\hat{\psi} = -c_s^2 \frac{k}{\mathcal{H}}\delta - (1 + w)\frac{k}{\mathcal{H}}\alpha \quad (3.17)$$

$$\left(\frac{k}{\mathcal{H}}\right)^2 \alpha = -\frac{3}{2}(1 + 3c_s^2)\delta. \quad (3.18)$$

In the case of the QCD transition, the transition time is short compared to the Hubble time ( $t_+ - t_-$ )  $< t_H = H^{-1}$  and therefore self-gravity of the dominant radiation fluid can be neglected in the Euler equation (3.17) for this component. On the other hand, CDM moves in the external gravitational potential provided by the radiation fluid, and is coupled to the radiation fluid via the gravity term in the Euler equation. Therefore we have to keep the gravity term in the CDM Euler equation.

For a purely radiation dominated universe  $w = c_s^2 = \frac{1}{3}$ , the solution for the density contrast  $\delta$  and the peculiar velocity  $\hat{\psi}$  can be written in terms of spherical Bessel and Neumann functions [44]

$$\delta = x f(x) + \frac{3}{x^2 + 6} x^2 \frac{d}{dx} f(x) \quad (3.19)$$

$$\hat{\psi} = \frac{1}{x^2 + 6} x^3 \frac{d}{dx} f(x), \quad (3.20)$$

where  $x \equiv k_{\text{phys}}/H = k/\mathcal{H}$ . For a radiation dominated universe  $x = k\eta$ ,  $f(x) \equiv [A j_1(x/\sqrt{3}) + B n_1(x/\sqrt{3})]/\sqrt{3}$ . The normalization is chosen in such a way that the subhorizon modes,  $\lambda^{\text{phys}} \ll H^{-1}$ , of  $\delta$  and  $\sqrt{3}\hat{\psi}$  are acoustic oscillations with constant amplitude  $\sqrt{A^2 + B^2}$ . We will fix our initial conditions to be the growing mode in the radiation dominated superhorizon regime,

$$\delta = A \frac{1}{6} x^2 \quad (3.21)$$

$$\hat{\psi} = A \frac{1}{54} x^3. \quad (3.22)$$

## B. Numerical results

The transfer functions for the radiation fluid and the cold dark matter are calculated by integrating the exact general relativistic set of equations (3.10)–(3.12) throughout the QCD transition. The initial conditions are fixed at  $T = 100 \text{ GeV}$ , where all scales under considerations were far above the horizon. We fix the initial amplitude of the radiation fluid,  $A_{\text{in}}$ , by the growing mode of an exactly radiation dominated solution, Eqs. (3.21) and (3.22). The normalization constant is given by the COBE normalized [45] Harrison-Zel'dovich spectrum [13], but it drops out in the transfer functions. The initial conditions for CDM are obtained assuming adiabatic perturbations; i.e., the entropy per cold particle is unperturbed  $\delta(s^{\text{RAD}}/n^{\text{CDM}}) = 0$ . Since  $\rho^{\text{CDM}}$

$= mn^{\text{CDM}} \propto 1/V_{\text{comoving}}$  and  $\rho^{\text{RAD}} \propto (1/V_{\text{comoving}})^{4/3}$ , the adiabatic initial conditions for  $\delta^{\text{CDM}}$  can be written

$$\delta^{\text{CDM}} = \frac{3}{4} \delta^{\text{RAD}}. \quad (3.23)$$

The initial fluid velocities are equal. Since we are in the linear regime, each spatial Fourier mode evolves independently.

For a first-order phase transition it is convenient to use the volume of a comoving box  $\propto a^3$  instead of time as the evolution variable. Thus, the derivatives in Eqs. (3.10) and (3.11) have to be replaced,  $\mathcal{H}^{-1}(d/d\eta) = a(d/da)$ . In Secs. II C and II D we have given  $w$  and  $c_s^2$  in terms of the scale factor. In the case of a crossover we use the temperature  $T$  as the independent evolution variable, since temperature is decreasing strictly monotonically in time. The derivatives in Eqs. (3.10) and (3.11) are replaced by  $\mathcal{H}^{-1}(d/d\eta) = -3c_s^2 T(d/dT)$ . We obtain  $p(T)$  by integrating the entropy density  $s(T)$ , Eq. (2.2).

The transfer functions are evaluated by evolving each mode from the initial temperature  $T_{\text{in}} = 100 \text{ GeV}$  to the final temperature  $T_f = T_*/10 = 15 \text{ MeV}$ , i.e. until the peculiar velocity of CDM has redshifted away. At  $T_f$  the universe is exactly radiation dominated. The amplitude of the acoustic oscillations is  $A^{\text{RAD}} \equiv (\delta_{\text{RAD}}^2 + 3\hat{\psi}_{\text{RAD}}^2)^{1/2}$ . The final amplitude of CDM is  $A^{\text{CDM}} = |\delta^{\text{CDM}}|$ . The transfer functions for the radiation and the CDM fluid are defined by

$$\mathcal{T}^{\text{RAD}}(k, \text{in} \rightarrow \text{f}) \equiv \frac{A^{\text{RAD}}(k)|_{T_f}}{A_{\text{in}}} \quad (3.24)$$

$$\mathcal{T}^{\text{CDM}}(k, \text{in} \rightarrow \text{f}) \equiv \frac{A^{\text{CDM}}(k)|_{T_f}}{A_{\text{in}}}, \quad (3.25)$$

where  $A_{\text{in}} = A_{\text{in}}^{\text{RAD}}$ .

For the bag model the transfer functions are shown in Fig. 5. Both transfer functions show huge peaks on small scales. The different scales  $k = 2\pi/\lambda$  are represented by the invariant CDM mass contained in a sphere with radius  $\lambda/2$ ,

$$M^{\text{CDM}}(\lambda^{\text{phys}}) \equiv \frac{4\pi}{3} \rho^{\text{CDM}} \left(\frac{\lambda^{\text{phys}}}{2}\right)^3, \quad (3.26)$$

assuming that  $\Omega_{\text{CDM}} \approx 1$  today. The largest scales in Fig. 5 correspond to the horizon at  $T_f = T_*/10$ . The CDM curve also shows the logarithmic growth of subhorizon scales of CDM in a radiation dominated universe. The CDM peaks lie on top of this logarithmic curve.

The peak structure starts at a scale  $\approx 10^{-8} M_{\odot}$  in CDM mass. This scale corresponds to the horizon scale at the QCD transition,  $M_H \equiv (4\pi/3)\rho^{\text{CDM}}(R_H/2)^3$ . The radiation energy inside the horizon at  $T_*$  is  $\sim 1 M_{\odot}$ , but it is redshifted as  $M^{\text{RAD}}(a) \sim (a_{\text{equality}}/a) M^{\text{CDM}}$ . Scales which are above the horizon at the QCD transition are not affected in accordance with the general proof in the previous section, Eq. (3.15). For scales below  $M_1^{\text{CDM}} \approx 9 \times 10^{-9} M_{\odot}$  the radiation peaks grow linearly in wave number. This linear growth comes from the

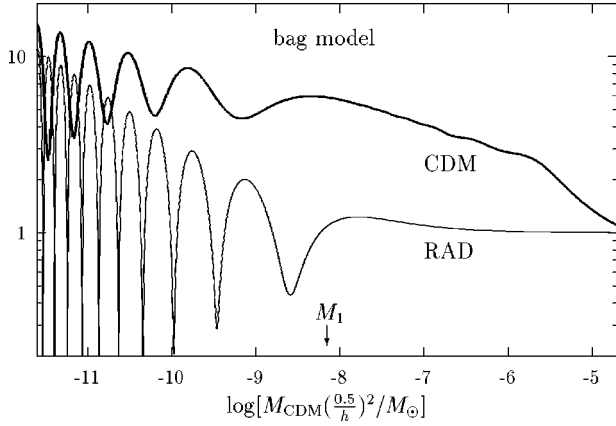


FIG. 5. The modifications of the density contrast for kinetically decoupled CDM (like axions or primordial black holes),  $A^{\text{CDM}} \equiv |\delta^{\text{CDM}}|(T_*/10)$ , and of the radiation fluid amplitude  $A^{\text{RAD}} \equiv (\delta_{\text{RAD}}^2 + 3\hat{\psi}_{\text{RAD}}^2)^{1/2}$  due to the QCD transition in the bag model. Both quantities are normalized to the pure Harrison-Zel'dovich radiation amplitude. On the horizontal axis the wave number  $k$  is represented by the CDM mass contained in a sphere of radius  $\pi/k$ .

fact that the vanishing sound speed during the QCD transition implies a vanishing restoring force in the acoustic oscillations on subhorizon scales. Therefore, the radiation fluid falls freely during the transition, with a constant velocity given at the beginning of the transition. The density contrast  $\delta^{\text{RAD}}$  grows linearly in time with a slope  $k$ . CDM is moving in an external potential provided by the dominant radiation fluid, and is pushed by the strong increase in the gravitational force during the transition. The highest peaks have  $k/k_1 \sim 10^4$ , because on smaller scales the acoustic oscillations are damped away by neutrino diffusion already before the QCD transition (see Sec. IV).

For our fit to lattice QCD the transfer functions  $\mathcal{T}^{\text{RAD}}, \mathcal{T}^{\text{CDM}}$  are shown in Fig. 6. The peak structure starts at the horizon scale  $M_1$ , but the asymptotic growth on small scales is different. It grows  $\propto k^{3/4}$  starting at a scale  $k_2$  which corresponds to an invariant CDM mass of  $M_2 = 2 \times 10^{-10} M_\odot$ . The asymptotic envelope for small scales is indicated by the straight line in Fig. 6. The highest peaks

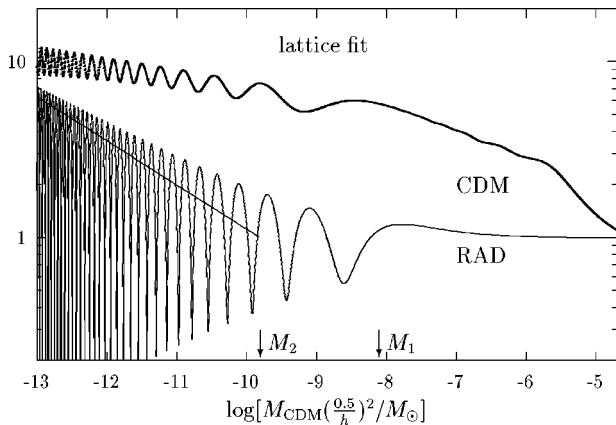


FIG. 6. The same as Fig. 5, but for our lattice QCD fit. The straight line denotes the asymptotic envelope for small scales  $\propto k^{3/4}$ .

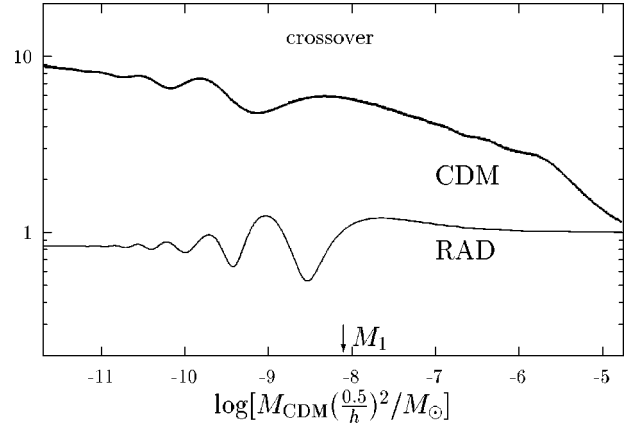


FIG. 7. The same as Fig. 5, but for a QCD crossover.

show an amplification of a factor 400 and correspond to wave numbers  $k/k_2 \sim 3 \times 10^3$ . The smaller amplification compared to the bag model is due to the decrease of the radiation fluid velocity before the transition. This happens because the sound speed drops below  $1/\sqrt{3}$  already before the transition. The values for  $M_2$  and the exponent of asymptotic growth depend on our specific choice of the latent heat ( $R_L = 0.2$ ) and the thermodynamic behavior at  $T > T_*$ , parametrized by  $\gamma$  ( $\gamma = 1/3$ ). In the next section we will show that the exponent of the asymptotic envelope for  $\gamma \in (0, 1)$  varies between  $1/2$  and  $1$ .

The processed spectrum for a crossover, Fig. 7, shows a similar behavior as for the bag model and the lattice fit on superhorizon and horizon scales. The peak structure starts at  $M_1$ , but on subhorizon scales there are no peaks. The level of the subhorizon transfer function for the radiation fluid is reduced to 0.83. This comes from the damping of the acoustic oscillations during the time with  $c_s^2 \neq 1/3$ .

### C. Analytic solution for the radiation fluid

The time evolution for subhorizon modes,  $\lambda^{\text{phys}} \ll R_H = H^{-1}$ , at the transition can be solved analytically. For the dynamics of the radiation fluid (QCD, photons, leptons) one can neglect cold dark matter, since  $\rho^{\text{CDM}}/\rho^{\text{RAD}} = a/a_{\text{equality}} \approx 10^{-8}$ . The transition time is short compared to the Hubble time at the transition,  $(t_+ - t_-) < t_H = H^{-1}$ . For subhorizon modes we can neglect gravity during the whole transition as we will show below. The damping terms in the continuity equation (3.16) and Euler equation (3.17) are absent in the purely radiation dominated regime. During the transition the damping terms can be neglected in view of the huge amplification for a first-order phase transition. Equations (3.16) and (3.17) now read

$$\begin{aligned} \delta' - k\hat{\psi} &= 0 \\ \hat{\psi}' + c_s^2 k\delta &= 0. \end{aligned} \quad (3.27)$$

Written as a second order differential equation for  $\delta$ , this is just an oscillator equation

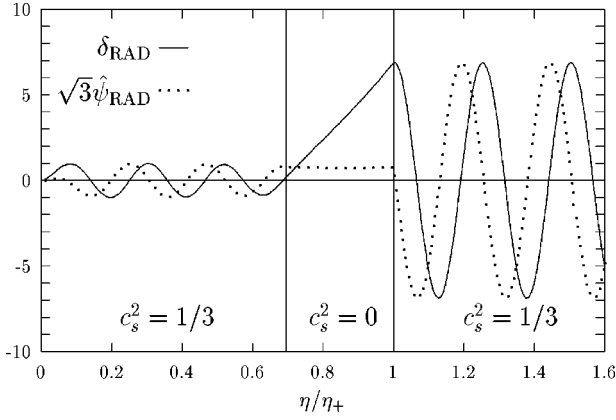


FIG. 8. The time evolution of the density contrast,  $\delta^{\text{RAD}}$ , and the peculiar velocity,  $\frac{\sqrt{3}}{4}\hat{\psi}^{\text{RAD}}$ , of the radiation fluid for the mode  $k/k_1 = 7$  in the uniform expansion gauge. During the QCD transition in the bag model—marked by the 2 vertical lines—the velocity stays approximately constant and the density contrast grows linearly. The amplitude is normalized to 1 long before the transition.

$$\delta' + \omega^2 \delta = 0, \quad (3.28)$$

with the time-dependent frequency  $\omega(\eta) \equiv kc_s(\eta)$ .

### 1. Bag model

We first discuss the origin of large amplifications for small scales in the bag model. Before and after the QCD transition the radiation fluid makes standing acoustic oscillations in each mode  $k$  with sound speed  $c_s^2 = 1/3$  and with amplitude  $A_{\text{in}}$  and  $A_{\text{out}}$  for the incoming and outgoing solution respectively; see Fig. 8. The incoming solution for the density contrast  $\delta$  and the peculiar velocity  $\sqrt{3}\hat{\psi}$  reads

$$\begin{aligned} \delta &= -A_{\text{in}} \cos[\omega(\eta - \eta_-) + \varphi_-] \\ \sqrt{3}\hat{\psi} &= A_{\text{in}} \sin[\omega(\eta - \eta_-) + \varphi_-]. \end{aligned} \quad (3.29)$$

This solution is valid until the beginning of the transition at  $\eta = \eta_-$ , and  $\varphi_-$  denotes the phase of the oscillation at  $\eta_-$ . During the transition the sound speed is zero. There are no restoring forces from pressure gradients and the radiation fluid falls freely. Since the duration of the transition is short compared to the Hubble time  $\Delta t \equiv (t_+ - t_-) < H^{-1}$ , gravity is negligible during this free fall. If we estimate the contribution of the gravity term in the Euler equation (3.17) during the transition, we get  $(t_+ - t_-)\partial_t \hat{\psi}_- = \mathcal{O}(\Delta t k_{\text{phys}}) \alpha_- = \mathcal{O}[(H\Delta t)(H/k_{\text{phys}})] \delta_- = \mathcal{O}[(H\Delta t)(H/k_{\text{phys}})] \hat{\psi}_- \ll \hat{\psi}_-$  except for an initial phase  $\varphi_- = 0 \bmod \pi$  (which leads to a dip in the spectrum). Thus, the fluid is moving inertially in the sense of Newton, the velocity stays constant, and the density contrast grows linearly in time,

$$\begin{aligned} \delta &= \delta_- + k(\eta - \eta_-)\hat{\psi}_-, \\ \sqrt{3}\hat{\psi} &= \sqrt{3}\hat{\psi}_-, \end{aligned} \quad (3.30)$$

where  $\sqrt{3}\hat{\psi}_- = A_{\text{in}} \sin(\varphi_-)$  is the peculiar velocity at  $\eta_-$ .

Since we have no jumps in pressure  $p_0$ , the density contrast  $\delta$  and the fluid velocity  $\hat{\psi}$  stay continuous throughout the whole transition, in particular at the matching points of the different regimes. Gravity remains negligible during the entire transition since the growth of  $\hat{\psi}$  due to gravity at the end of the transition can be estimated by  $\hat{\psi}_+ - \hat{\psi}_- = \mathcal{O}(\Delta t k_{\text{phys}} \alpha_+) = \mathcal{O}[H\Delta t(H/k_{\text{phys}})\delta_+] = \mathcal{O}[(H\Delta t)^2 \hat{\psi}_-] \ll \hat{\psi}_-$ , in the limit under consideration. At the end of the transition this solution has to be joined to the pure radiation dominated regime for  $T \leq T_*$ . Since the amplitude of the density contrast grows linearly during the transition, the final amplitude  $A_{\text{out}} = A_+$  is enhanced linearly in  $k$ , modulated by the incoming phase

$$\left(\frac{A_{\text{out}}}{A_{\text{in}}}\right)^2 = \left(\frac{k}{k_1}\right)^2 \sin^2(\varphi_-), \quad (3.31)$$

with  $k_1 \equiv \sqrt{3}/\Delta\eta$ ,  $\Delta\eta \equiv \eta_+ - \eta_-$ . The envelope of the linearly growing peak structure for subhorizon scales starts at the scale  $k_1$  which corresponds to a CDM mass of  $M_1 = 9 \times 10^{-9} M_\odot$ .

### 2. Lattice QCD

For our fit to lattice QCD, Eq. (2.8), the time evolution separates into four regimes. First we have a WKB regime, where the sound speed is slowly changing compared to the frequency of the oscillation; i.e., the WKB condition  $|dc_s/d\eta|/c_s \ll \omega = kc_s$  is satisfied. The WKB solution is

$$\begin{aligned} \delta &= -\frac{A_{\text{in}}}{(3c_s^2)^{1/4}} \cos \int_0^\eta \omega(\eta') d\eta' \\ \sqrt{3}\hat{\psi} &= A_{\text{in}} (3c_s^2)^{1/4} \sin \int_0^\eta \omega(\eta') d\eta', \end{aligned} \quad (3.32)$$

where  $A_{\text{in}}$ , as before, denotes the incoming subhorizon amplitude in a radiation dominated universe. The decreasing sound speed in the WKB regime leads to an increase in the density contrast and a decrease in peculiar velocity compared to the purely radiation dominated case. Close to  $\eta_-$  the WKB condition can no longer be satisfied: Since  $c_s$  decreases by some power in  $(\eta_- - \eta)$ , Eq. (2.25), the left hand side of the WKB condition diverges like  $1/(\eta_- - \eta)$ , whereas the right hand side for any fixed  $k$  goes to zero. Therefore, the WKB solution for a given mode is valid up to a certain time  $\tilde{\eta}(k) < \eta_-$ .  $\tilde{\eta}(k)$  approaches  $\eta_-$  for increasing  $k$ .

Close to  $\eta_-$  there is a second regime (overlapping with the WKB regime for large enough  $k$ ), where  $c_s$  can be approximated by the power law of Eq. (2.25),

$$\begin{aligned} c_s &= C \left( \frac{\eta_- - \eta}{\eta_-} \right)^{1/(2\beta) - 1} \\ \beta &\equiv \frac{\gamma}{\gamma + 1}, \end{aligned} \quad (3.33)$$

where  $\beta$  is defined for convenience below. Inserting this power law into the oscillator equation (3.28) gives a Bessel differential equation. The new variable  $z$  is the argument of the cosine in the WKB expansion,

$$z \equiv k \int_{\eta}^{\eta_-} c_s(\eta') d\eta' = 2C\beta(k\eta_-) \left( \frac{\eta_- - \eta}{\eta_-} \right)^{1/(2\beta)}. \quad (3.34)$$

The index  $\bar{\beta}$  of the Bessel functions is obvious from the ratio of the two fundamental solutions  $J_{\bar{\beta}}(z)/N_{\bar{\beta}}(z) \propto z^{2\bar{\beta}} \propto (\eta_- - \eta)^{\bar{\beta}/\beta}$ . Since the two fundamental solutions for  $c_s \rightarrow 0$  are  $\delta \rightarrow \text{const}$  and  $\delta \propto (\eta_- - \eta)$ , it follows that  $\bar{\beta} = \beta$ . The prefactor must be  $z^\beta$  to make the second fundamental solution constant,

$$\delta = z^\beta [-B_1 J_\beta(z) + B_2 N_\beta(z)]. \quad (3.35)$$

The peculiar velocity follows via  $\hat{\psi} = \delta'/k$ ; see Eq. (3.27). Matching the WKB solution with the Bessel solution in the overlap region  $z \gg 1$ , where  $J_\beta(z), N_\beta(z) \rightarrow \sqrt{2/(\pi z)} \cos[z - (\pi/2)(\beta + 1/2, 3/2)]$ , gives the normalization  $B^2 \equiv B_1^2 + B_2^2$ ,

$$B = A_{\text{in}} \frac{\sqrt{\pi\beta}}{3^{1/4}} (2C\beta)^{-\beta} (k\eta_-)^{1/2-\beta}. \quad (3.36)$$

At the beginning of the first-order transition,  $\eta = \eta_-$ , the Bessel solution (second regime) is matched to the third regime, i.e. the free fall regime with  $c_s^2 = 0$ . As in the bag model, peaks in the transfer function for large  $k$  are obtained for the mixing angles  $\varphi$  in the Bessel solution ( $B_1 = B \cos \varphi, B_2 = B \sin \varphi$ ) which give the maximal  $|\hat{\psi}|$  at the matching point. With  $J_\beta(z) \rightarrow (z/2)^\beta / \Gamma(\beta + 1)$  for  $z \ll 1$  and  $N_\beta(z) = [J_\beta(z) \cos(\beta\pi) - J_{-\beta}(z)] / \sin(\beta\pi)$  we find

$$\hat{\psi}_{-}^{\text{max}} = A_{\text{in}} \frac{\sqrt{\pi\beta}}{3^{1/4}} \frac{(C\beta)^\beta}{\Gamma(\beta + 1) \sin \beta\pi} (k\eta_-)^{\beta-1/2}. \quad (3.37)$$

The evolution in the third regime,  $c_s^2 = 0$ , is as before. The restoring force in the oscillator equation (3.28) vanishes, the fluid moves with constant peculiar velocity,  $\hat{\psi}(\eta) = \hat{\psi}_-$ , and the density contrast grows linearly in time.

After the transition ( $\eta > \eta_+$ , fourth regime) the universe is radiation dominated ( $c_s^2 = 1/3$ ) and the solutions are oscillations with amplitude  $A_{\text{out}} = A_+$ . The amplification of peaks in the outgoing amplitude  $A_{\text{out}}$  is given by  $A_{\text{out}}|_{\text{peaks}} = \hat{\psi}_{-}^{\text{max}} k \Delta \eta$ ,

$$\frac{A_{\text{out}}}{A_{\text{in}}}|_{\text{peaks}} = \frac{\sqrt{\pi\beta}}{3^{1/4}} \frac{(C\beta)^\beta}{\Gamma(\beta + 1) \sin \beta\pi} (k\eta_-)^{\beta-1/2} k \Delta \eta. \quad (3.38)$$

The dependence on the latent heat is encoded in the duration  $\Delta \eta$  of the transition.  $C$  and  $\beta$  are determined by the normalization and the power law for  $c_s(\eta)$  shortly before the onset

of the first-order phase transition, Eq. (3.33). Replacing  $\beta$  by  $\gamma$  (=the exponent in the QCD fit to the entropy density) the amplification factor is

$$\frac{A_{\text{out}}}{A_{\text{in}}}|_{\text{peaks}} = \left( \frac{k}{k_2} \right)^{(3\gamma+1)[2(\gamma+1)]} \quad (3.39)$$

for large  $k$ . Since  $0 < \gamma < 1$ , the exponent of the power law varies between 1/2 and 1. The normalization of the peak amplification for large  $k$  is encoded in  $k_2$ . In our fit to lattice QCD we take  $\gamma = 1/3$ , and hence  $\beta = 1/4$ ,

$$\frac{A_{\text{out}}}{A_{\text{in}}}|_{\text{peaks}} = \left( \frac{k}{k_2} \right)^{3/4}. \quad (3.40)$$

For  $R_L = 0.2$ ,  $k_2$  corresponds to a CDM mass of  $M_2 = 2 \times 10^{-10} M_\odot$ . The spectrum for this case together with the asymptotic envelope is plotted in Fig. 6.

### 3. Crossover

In the case of a crossover, the amplification is occurring for scales around the Hubble radius at the transition only. Subhorizon scales always stay in the WKB-regime and therefore the spectrum is flat for these scales. However, the amplitude for subhorizon scales is damped during the phase transition. The same damping occurs in the case of a first-order phase transition. It has been neglected in the analytic discussion, since it is a small correction. The time evolution of the density contrast of subhorizon scales, including damping terms, reads

$$\delta'' + (1 + 3c_s^2 - 6w) \frac{a'}{a} \delta' + \omega^2(\eta) \delta = 0. \quad (3.41)$$

The friction term in this equation can be eliminated if we write the density contrast as  $\delta = [(\sqrt{1+w})/a'] u(\eta)$ . Inserting this ansatz into Eq. (3.41), using the Friedmann equation and  $w' = 3aH(1+w)(w - c_s^2)$ , we obtain an undamped oscillator equation with frequency  $\omega(\eta) = kc_s(\eta)$  for the quantity  $u(\eta)$ . For a crossover the sound velocity never vanishes, and subhorizon modes always satisfy the WKB-condition. Therefore, we obtain, for the density contrast and the peculiar velocity,

$$\begin{aligned} \delta &= - \frac{A_{\text{in}}}{(3c_s^2)^{1/4}} \frac{a'_{\text{in}}}{a'} \frac{\sqrt{3(1+w)}}{2} \cos \int \omega(\eta) d\eta \\ \hat{\psi} &= A_{\text{in}} (3c_s^2)^{1/4} \frac{a'_{\text{in}}}{a'} \frac{\sqrt{3(1+w)}}{2} \sin \int \omega(\eta) d\eta. \end{aligned} \quad (3.42)$$

The reduction of the amplitude of subhorizon scales is given by

$$\frac{A_{\text{out}}}{A_{\text{in}}} = \frac{(Ha^2)_{\text{in}}}{(Ha^2)_{\text{out}}} = \left( \frac{g_+}{g_-} \right)^{1/6}. \quad (3.43)$$

Therefore the subhorizon amplitudes are reduced to 83% of their initial value. This damping is a general feature appear-

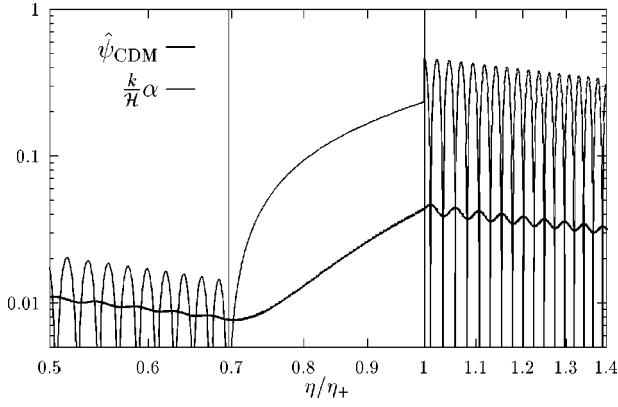


FIG. 9. The time evolution of the peculiar velocity,  $\hat{\psi}_{\text{CDM}}$ , of the kinetically decoupled cold dark matter fluid (axions or primordial black holes) and the external gravitational potential gradient  $(k_{\text{phys}}/H)\alpha$  for the mode  $k/k_1=37$  in the uniform expansion gauge.  $\alpha$  is provided by the radiation fluid. During the QCD transition in the bag model—marked by the 2 vertical lines—the cold dark matter fluid is accelerated by the gravitational force.

ing whenever the number of degrees of freedom is reduced. Also in the case of a first-order transition, this damping factor should be taken into account. However, it changes the huge amplifications merely by the constant factor 0.83.

#### D. Analytic solution for CDM

Cold dark matter is assumed to be the major matter content of the universe today. At the time of the QCD transition, however, the contribution of CDM to the total energy density was negligible,  $\rho^{\text{CDM}}/\rho^{\text{RAD}}=a/a_{\text{equality}}\approx 10^{-8}$ . We consider a type of CDM which is non-relativistic ( $p\ll\rho$ ) at the QCD transition and which is only coupled via gravity to the radiation fluid. CDM moves in the external gravitational potential provided by the dominant radiation fluid. During the QCD transition, the big amplifications of the density contrast in the radiation fluid  $\delta^{\text{RAD}}$  leads to a big amplification in the gravitational potential, i.e., the force term in the Euler equation for CDM. The CDM is accelerated to higher velocities at the end of the transition. Therefore, we also get peaks and dips in the cold dark matter fluid.

The subhorizon evolution of CDM in a purely radiation dominated universe is just inertial motion. This can be seen from the Euler equation (3.17): The sound velocity of cold dark matter is zero,  $c_s^2\equiv 0$ , and the gravitational potential  $\alpha$  is given using the Poisson equation (3.18) for the dominant density contrast  $\delta^{\text{RAD}}$ , Eq. (3.30). In the leading order in  $x=k/\mathcal{H}$ , the gravitational force can be neglected and the subhorizon evolution of the CDM velocity is obtained:

$$\hat{\psi}_{\text{CDM}}=C\frac{1}{x}. \quad (3.44)$$

The velocity of CDM in a radiation dominated universe just redshifts to zero on subhorizon scales; see Fig. 9. Here  $C$  is an integration constant of order  $A_{\text{in}}$ . The corresponding evolution of the density contrast  $\delta^{\text{CDM}}$  follows from the continuity equation (3.16),

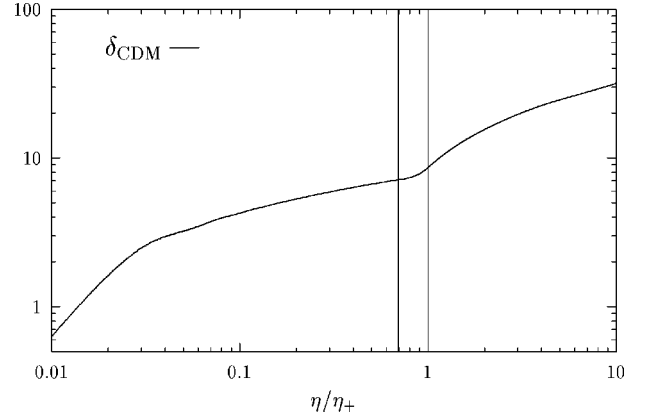


FIG. 10. The time evolution of the CDM density contrast,  $\delta^{\text{CDM}}$ , corresponding to the CDM velocity of Fig. 9. The major amplification of  $\delta^{\text{CDM}}$  is due to the higher peculiar velocity at the end of the transition.

$$\delta^{\text{CDM}}=C\ln x+D. \quad (3.45)$$

This logarithmic growth of  $\delta^{\text{CDM}}$  can be seen in Fig. 10 before and after the transition. The shape of  $\delta^{\text{CDM}}$  can also be seen in the transfer functions, Figs. 5, 6, 7 on scales above the horizon scale  $M_1$ .

During a first-order QCD transition the evolution of the gravitational potential is dominated by the linear growth in time of  $\delta^{\text{RAD}}$ , Eq. (3.30). From the Poisson equation (3.18) it follows that the gravitational potential grows linearly in time,

$$\alpha=-\frac{3}{2}\mathcal{H}(\eta-\eta_-)\left(\frac{\mathcal{H}}{k}\right)\hat{\psi}_{-}^{\text{RAD}}; \quad (3.46)$$

see Fig. 9. As before, we will take the transition time to be short compared to the Hubble time  $\Delta t<H^{-1}$ ; hence  $\Delta\eta<\mathcal{H}^{-1}$ . The gravitational force in the Euler equation (3.17) and hence the fluid acceleration for CDM also grow linearly in time during the transition. The fluid velocity grows quadratically,

$$\hat{\psi}_{+}^{\text{CDM}}=\frac{3}{4}[\mathcal{H}\Delta\eta]^2\hat{\psi}_{-}^{\text{RAD}}+\hat{\psi}_{-}^{\text{CDM}}. \quad (3.47)$$

The initial CDM velocity  $\hat{\psi}_{-}^{\text{CDM}}$  is given by Eq. (3.44). On scales well below the horizon the velocity is redshifted to small values and can be neglected. However, on subhorizon scales closer to the horizon the initial velocity dominates, because  $[\mathcal{H}(\Delta\eta)]^2\approx 0.1(0.01)$  for the bag model (lattice fit) is small. According to the continuity equation (3.16) the density contrast  $\delta^{\text{CDM}}$  grows cubically:

$$\delta_{+}^{\text{CDM}}=\delta_{-}^{\text{CDM}}+\frac{1}{4}\left(\frac{k}{\mathcal{H}}\right)[\mathcal{H}\Delta\eta]^3\hat{\psi}_{-}^{\text{RAD}}. \quad (3.48)$$

Because of the cube, the growth of  $\delta^{\text{CDM}}$  during the QCD transition is small.

The major amplification effect comes from the higher velocity at the end of the transition (see Fig. 9), which leads to

$$\delta^{\text{CDM}}(\eta) = \hat{\psi}_+^{\text{CDM}} k \eta_+ \ln\left(\frac{\eta}{\eta_+}\right) + \delta_+^{\text{CDM}}. \quad (3.49)$$

The amplification of the density contrast during the transition is negligible compared to the enhancement of the velocity. This velocity enhancement during the transition leads to an additional logarithmic growth of  $\delta^{\text{CDM}}$  after the transition,

$$\delta^{\text{CDM}}(\eta) = \left[ \frac{3}{4} \left( \frac{\Delta\eta}{\eta_+} \right)^2 \hat{\psi}_-^{\text{RAD}} \right] k \eta_+ \ln\left(\frac{\eta}{\eta_+}\right) + \delta_+^{\text{CDM}}. \quad (3.50)$$

Here we have used Eq. (3.47) to obtain the leading subhorizon approximation. This additional logarithmic growth of  $\delta^{\text{CDM}}$  is most clearly seen in Fig. 10.

The number of CDM peaks in the numerical result, Figs. 5–7, is only half of the radiation peaks. This comes from the fact that the peaks in  $\delta^{\text{CDM}}$  lie on top of the logarithmic curve, which is still the main contribution at the scales plotted. The dips correspond to modes, with a maximal negative amplification.

The jump in the gravitational potential at the end of the QCD transition in Fig. 9 follows from the Poisson equation (3.18). Since  $\delta$  is continuous, but  $c_s^2$  jumps, the right hand side abruptly changes by a factor of 2. Therefore  $\alpha$  jumps by the same factor.

Let us compare the ‘‘QCD peaks’’ in the CDM spectrum with the CDM spectrum without phase transition. In the limit  $\rho^{\text{CDM}}/\rho^{\text{RAD}} \ll 1$  the exact solution to Eqs. (3.10)–(3.12) in the radiation dominated universe without transition reads ( $x = k/\mathcal{H}$ ):

$$\delta^{\text{CDM}} = \frac{3A_{\text{in}}}{2} \left\{ \ln\left(\frac{x}{\sqrt{3}}\right) + \gamma_E - \frac{1}{2} - \text{Ci}\left(\frac{x}{\sqrt{3}}\right) + \frac{3}{x^2+6} \left[ \frac{x}{\sqrt{3}} \sin\left(\frac{x}{\sqrt{3}}\right) + \cos\left(\frac{x}{\sqrt{3}}\right) \right] \right\} \quad (3.51)$$

$$\hat{\psi}^{\text{CDM}} = \frac{3A_{\text{in}}}{2x} \left\{ 1 - \frac{6}{x^2+6} \left[ \frac{x}{\sqrt{3}} \sin\left(\frac{x}{\sqrt{3}}\right) + \cos\left(\frac{x}{\sqrt{3}}\right) \right] \right\}. \quad (3.52)$$

In the subhorizon limit this solution reduces to

$$\delta^{\text{CDM}} = \frac{3A_{\text{in}}}{2} \left[ \ln\left(\frac{x}{\sqrt{3}}\right) + \underbrace{\gamma_E - \frac{1}{2}}_{\approx 0.077} \right] \quad (3.53)$$

$$\hat{\psi}^{\text{CDM}} = \frac{3A_{\text{in}}}{2} \frac{1}{x}, \quad (3.54)$$

which fixes the constants  $C$  and  $D$  in Eqs. (3.44) and (3.45).

We are now able to calculate the enhancement factor

$$\mathcal{E}(\eta) \equiv \left[ \frac{\delta_{\text{transition}}}{\delta_{\text{no transition}}} \right]^{\text{CDM}}(\eta). \quad (3.55)$$

Let us evaluate  $\mathcal{E}$  at equality, i.e.,  $\eta_{\text{eq}}/\eta_+ \approx 2 \times 10^8$ :

$$\mathcal{E}(\eta_{\text{eq}}) \approx 1 + \left[ \frac{1}{2} \left( \frac{\Delta\eta}{\eta_+} \right)^2 \hat{\psi}_-^{\text{RAD}} \right] k \eta_+ \ln\left(\frac{\eta_{\text{eq}}}{\eta_+}\right) / \ln\left(\frac{k \eta_{\text{eq}}}{\sqrt{3}}\right). \quad (3.56)$$

The enhancement at the smallest scales  $M^{\text{CDM}} \sim 10^{-20} M_\odot$  to which our calculation applies and at some intermediate scale  $M^{\text{CDM}} \sim 10^{-15} M_\odot$  reads

$$\mathcal{E}(\eta_{\text{eq}}) \approx \begin{cases} 600(20) & \text{bag model} \\ 10(2) & \text{lattice fit} \end{cases} \quad \text{for } 10^{-20}(10^{-15}) M_\odot, \quad (3.57)$$

where we have used Eq. (3.37) for the case of the lattice fit. This shows that both models lead to large enhancements of the CDM density contrast at equality for small enough scales. For the lattice fit the enhancement becomes important at scales below  $M^{\text{CDM}} \sim 10^{-15} M_\odot$ .

## IV. IMPLICATIONS: CLUMPS IN CDM

### A. Fate of the peaks in the radiation fluid

Before discussing CDM, let us show that the large peaks in the density spectrum of the hadron-lepton-photon fluid do not lead to any observable consequences.

#### 1. Collisional damping at neutrino decoupling

The acoustic oscillations in the radiation fluid get damped by neutrino diffusion at the time of neutrino decoupling. This damping is analogous to Silk damping at photon decoupling. The muon and tau neutrinos, respectively, which are coupled to the RAD fluid via neutral current interactions only, decouple at  $T_{\nu_\mu \nu_\tau}^{\text{dec}} \sim 2.2$  MeV from the Hubble scale  $R_H$ , which follows from Ref. [46]. The electron neutrinos interact by charged and neutral currents and decouple slightly later,  $T_{\nu_e}^{\text{dec}} \sim 1.4$  MeV. By the time of neutrino decoupling at the Hubble scale all inhomogeneities in the RAD fluid on scales below  $\approx 10^{-6} M_\odot$  in CDM mass are wiped out by neutrino diffusion (cf. the QCD horizon scale is  $10^{-8} M_\odot$  in CDM mass), as shown below, Eq. (4.5). Therefore our QCD peaks cannot affect BBN.

It is important to distinguish the total decoupling of neutrinos, i.e. neutrino decoupling at the Hubble scale, when the neutrino scattering rate  $\Gamma$  is less than the Hubble rate,  $\Gamma_\nu/H < 1$ , from the neutrino decoupling with respect to a certain mode given by  $\Gamma_\nu/\omega_{\text{phys}} < 1$ , when the typical neutrino scatters less than once during an acoustic oscillation time of one particular mode. The mode-dependent decoupling temperature  $T_\nu^{\text{dec}}(k)$  is related to the total decoupling temperature by

$$\frac{T_{\nu_i}^{\text{dec}}(k)}{T_{\nu_i}^{\text{dec}}(H)} \approx \left( \frac{c_s k_{\text{phys}}}{H} \right)_{T=T_{\nu_i}^{\text{dec}}(H)}^{1/4}. \quad (4.1)$$

This follows because the neutrino interaction rates  $\Gamma_{\nu}$  are proportional to  $T^5$  and  $k_{\text{phys}} \propto 1/a \propto T$ , and hence  $\Gamma_{\nu}/\omega_{\text{phys}} \propto T^4$ .

To compute the damping of acoustic oscillations in the radiation fluid by neutrino diffusion we follow Weinberg [47]. For a radiation fluid shear viscosity is dominant, bulk viscosity vanishes and heat conduction is negligible. The shear viscosity is given by

$$\eta_{\text{visc}} = \frac{4}{15} \sum_i \rho_{\nu_i} \tau_{\nu_i}. \quad (4.2)$$

$\rho_{\nu_i}$  denotes the energy density of a neutrino species;  $\tau_{\nu_i}$  is the typical collision time. In the subhorizon limit the Navier-Stokes equation and the continuity equation give

$$\delta'' + \frac{k_{\text{phys}}}{\rho_{\text{tot}}} \eta_{\text{visc}} k \delta' + \omega^2 \delta = 0, \quad (4.3)$$

a damped oscillator. The damping factor for the mode  $k$  at a given conformal time  $\eta$  is

$$D(k, \eta) = \exp \left[ -\frac{1}{2} \int_0^{\eta_{\text{max}}} (k_{\text{phys}}/\rho_{\text{tot}}) \eta_{\text{visc}} k d\eta' \right]. \quad (4.4)$$

Here the upper limit of the integral is the conformal time  $\eta_{\text{max}} = \text{Min}[\eta, \eta_{\text{dec}}(k)]$ , because collisional damping of the  $\gamma$ - $l^{\pm}$ -hadron fluid by neutrinos ceases at decoupling of the mode  $k$  considered. The damping per oscillation is largest for  $\omega \tau_{\nu} \equiv \omega/\Gamma_{\nu} \approx 1$ , i.e. immediately before neutrino decoupling for a given mode. But note that subhorizon modes get strongly damped long before the mode decouples from neutrinos, because a weak damping per oscillation is compensated by many oscillations per Hubble time.

For a first application we ask what modes are already damped by the time of the QCD transition. At the QCD transition,  $T = T_{\star}$ , the interaction rates for electron and muon neutrinos (respectively, antineutrinos) with the leptons are the same,  $\Gamma_{\nu_e} = \Gamma_{\bar{\nu}_e} = \Gamma_{\nu_{\mu}} = \Gamma_{\bar{\nu}_{\mu}} = 3.1 G_{\text{F}}^2 T^5$  [46], since electrons and muons are still relativistic. The  $\tau$ -neutrinos interact only via neutral currents with the leptons and have a lower interaction rate,  $\Gamma_{\nu_{\tau}} = \Gamma_{\bar{\nu}_{\tau}} = 0.6 G_{\text{F}}^2 T^5$ . Evaluating the damping integral, Eq. (4.4), at  $T = T_{\star}$  we find that the damping factor  $D(k, T_{\star})$  is  $< 1/e$  for  $(k_{\text{phys}}/H)_{T_{\star}} > 10^4$ , which corresponds to  $M_{\text{CDM}} < 10^{-20} M_{\odot}$ ; i.e., acoustic oscillations on these small scales are wiped out before the QCD transition. Therefore no peaks in the RAD or in the CDM transfer function can develop below this scale. This small-scale cutoff is independent of the bubble separation scale.

Next we consider  $T < T_{\nu_e}^{\text{dec}}(H) \approx 1.4 \text{ MeV}$  and evaluate the final damping factor  $D(k)$ . At the time of neutrino decoupling we take a purely radiation dominated universe, consisting of  $\gamma$ ,  $e^{\pm}$  and  $\nu$ 's only to evaluate the damping. Muons have disappeared since  $m_{\mu} \gg T$  and since  $\tau_{\mu} \ll t_{\text{H}}$ . The interaction rate for electrons is still given by charged and neutral currents,  $\Gamma_{\nu_e} = \Gamma_{\bar{\nu}_e} = 1.3 G_{\text{F}}^2 T^5$ , whereas muon and tau neutrinos have the same lower (neutral current) rate,  $\Gamma_{\nu_{\mu}} = \Gamma_{\bar{\nu}_{\mu}} = \Gamma_{\nu_{\tau}} = \Gamma_{\bar{\nu}_{\tau}} = 0.3 G_{\text{F}}^2 T^5$  [46]. The final damping of a certain scale (expressed in invariant CDM mass) from Eq. (4.4) is

$$D = \exp \left[ -\left( \frac{M_{\text{D}}}{M} \right)^{1/4} \right], \quad (4.5)$$

with the neutrino damping scale  $M_{\text{D}} \approx 1.9 \times 10^{-6} M_{\odot}$  in CDM mass. This is  $3 \times 10^{-5} M_{\text{H}}^{\text{CDM}}$  at  $T = 1.4 \text{ MeV}$  and corresponds to length scales  $\lambda = 1/30 R_{\text{H}}$ .

We conclude that the large peaks in the spectrum of the radiation fluid are damped away by the time of BBN. The large peaks in the RAD fluid generated by the QCD transition do not give a new mechanism for inhomogeneous BBN.

## 2. Black hole formation at the QCD transition?

It was suggested in the literature [49,19,50] that the QCD transition could lead to the formation of  $1 M_{\odot}$  black holes, which could account for dark matter today. Jedamzik [19] proposed to identify such black holes with the MACHOs observed by microlensing [22]. He pointed out that the formation of black holes should be particularly efficient during the QCD epoch due to the significant decrease in the effective sound speed.

In order to form a black hole in a radiation dominated universe, the density contrast inside the Hubble radius should be in the range  $1/3 < \delta_{\text{H}} < 1$  [51]. For an observable amount of  $1 M_{\odot}$  black holes today, i.e.  $\Omega_{\text{BH}}^{(0)} = \mathcal{O}(1)$ , the fraction of energy density converted to black holes at the QCD transition must be  $\mathcal{O}(a_{\text{QCD}}/a_{\text{equality}}) \approx 10^{-8}$ . For a Gaussian distribution this requires  $\delta_{\text{rms}} \approx 0.06$  (without including any enhancement from the QCD transition) [52]. The QCD transition gives an enhancement factor (at the horizon scale) of 2 for the bag model and of 1.5 for lattice QCD in our linear perturbation treatment, Figs. 5–7. This indicates a corresponding reduction in the required preexisting perturbation spectrum at the solar mass scale. Cardall and Fuller used a qualitative argument of Carr and Hawking [53] and the bag model and also obtained a factor of 2 reduction in the required preexisting perturbation spectrum [54]. These QCD factors of 1.5 or 2 are so modest that a preexisting Harrison-Zel'dovich spectrum with COBE normalization is very far from giving a cosmologically relevant amount of black holes [23]. One would have to put in a fine-tuned tilt ( $n-1$ )  $\approx 0.4$  to get the desired amount of black holes. However, this tilted spectrum would overproduce primordial black holes on scales which are only a factor 50 below the Hubble radius at the QCD transition. Therefore a break in the preexisting

spectrum below the QCD scale would be required, a second fine-tuning.

We conclude that the QCD transition enhances the probability of black hole formation, but the preexisting spectrum needs to be fine-tuned around the QCD scale and the major effect would not be due to the QCD transition.

## B. Kinetic decoupling of CDM

In Sec. III we established the generation of peaks in the CDM spectrum during a first-order QCD transition. Below, we discuss the properties of the most prominent CDM candidates at temperatures of the QCD scale. We show that weakly interacting massive particles, like the lightest supersymmetric particle or a heavy neutrino, are kinetically tightly coupled to the radiation fluid at the QCD transition and are included in the radiation fluid in our equations. Two CDM candidates that are kinetically decoupled from the radiation fluid and have  $p=0$  at the QCD epoch are the axion and primordial black holes. In our figures and equations kinetically decoupled CDM have been labeled by CDM for brevity.

### 1. Neutralinos and heavy neutrinos

We start our discussion with the lightest supersymmetric particle [20]. In the minimal supersymmetric standard model this is the neutralino (we assume it is stable). Constraints from LEP 2 and cosmology, together with the assumption of universality at the GUT scale, show that its mass is  $m_\chi > 42$  GeV [55]. It is essential to distinguish between the chemical freeze-out and the kinetic decoupling of neutralinos. The chemical freeze-out determines the amount of neutralinos today, and it happens when the annihilation rate of neutralinos drops below the Hubble rate,  $\Gamma_{\text{ann}}/H < 1$ . When the neutralinos become nonrelativistic the rate for neutralino annihilation,  $\Gamma_{\text{ann}} = \langle v \sigma_{\text{ann}} \rangle n_\chi$ , is suppressed by the Boltzmann factor in the number density of the neutralinos,  $n_\chi \sim (m_\chi T)^{3/2} \exp(-m_\chi/T)$ . The freeze-out temperature of the neutralino [20] is  $T_f \sim m_\chi/20 > 2$  GeV, and neutralinos are chemically decoupled at the QCD transition.

Kinetic decoupling, in contrast, is determined by the elastic scattering between neutralinos and the dominant radiation fluid. The interaction rate for elastic scattering is  $\Gamma_{\text{el}} = \tau_{\text{coll}}^{-1} = \langle v \sigma_{\text{el}} \rangle n$ , where  $n \sim T^3$  is the number density of relativistic particles, e.g. electrons or neutrinos. An order of magnitude estimate shows that  $\sigma_{\text{el}}$  is similar to the cross section for the elastic scattering of neutrinos and neutrons,  $\sigma_{\text{el}} \sim G_F^2 T^2$  [48]. We have to distinguish between the regime of perfect kinetic coupling, i.e. neutralinos tightly coupled to the radiation fluid, an intermediate regime where the neutralinos scatter elastically but the number of collisions is not sufficient to drag them along dissipationless, and the regime of kinetic decoupling,  $\Gamma_{\text{el}}/H < 1$ , which is roughly at  $T \lesssim 1$  MeV, since the neutralino interacts weakly.

Let us estimate the regime where the neutralinos belong to the perfect radiation fluid. Perfectness of a fluid (dissipationless) always refers to an external time scale,  $\omega^{-1}$  of an

acoustic oscillation or the Hubble time, etc. A fluid behaves as a perfect fluid, if  $\omega \tau_{\text{relax}} \ll 1$ ; i.e., the external time scale is larger than the relevant relaxation time, the fluid is continually in local thermal equilibrium, and no entropy production occurs. For the coupling of neutralinos to the radiation fluid the relaxation time is given by  $\tau_{\text{relax}} = N \tau_{\text{coll}}$ , where  $N$  is the number of collisions needed to completely change the momentum of the neutralino due to collisions with the radiation fluid. The momentum transfer at a collision of a lepton with the neutralino is of order  $p_1 \sim T$ . The kinetic energy of the neutralino is given by equipartition,  $p_\chi^2/2m_\chi \sim T$ ; hence its momentum is  $p_\chi \sim \sqrt{m_\chi T}$ . The fractional change of the neutralino momentum from one collision at the QCD transition is  $\delta p_\chi/p_\chi \sim \sqrt{T/m_\chi} \ll 1$ . After  $N$  collisions the total rms change of momentum is  $(\delta p_\chi/p_\chi)_{\text{rms}} \sim \sqrt{NT/m_\chi}$ . Local thermal equilibrium is obtained if the bulk motion of the neutralinos is governed by the leptons; i.e., the fractional change of the neutralino momentum is of order 1. The number of collisions needed to completely change direction is  $N \sim m_\chi/T \sim 300$  for  $m_\chi = 50$  GeV and  $T = T_*$ . The collision time is given by the weak interactions rate  $\Gamma_w = \tau_{\text{coll}}^{-1} \sim G_F^2 T_*^5$ , and the relaxation time is given by

$$\tau_{\text{relax}} = N \tau_{\text{coll}} \sim N \times 10^{-7} t_H, \quad (4.6)$$

with  $N \sim m_\chi/T$ . If we compare the relaxation time with the frequency of the acoustic oscillations, we find that the condition for a perfect fluid,  $\omega \tau_{\text{relax}} \ll 1$ , at the QCD transition is satisfied for scales  $\lambda > \lambda_{\text{dec}}(T_*) \approx 10^{-4} R_H$  ( $m_\chi = 50$  GeV). Hence the neutralinos on these scales are part of the radiation fluid at the QCD transition. Below this scale, the neutralinos cannot follow the acoustic oscillations. On the other hand, on the Hubble scale the perfect kinetic coupling of neutralinos to the radiation fluid stops when the required relaxation time becomes more than a Hubble time,  $\tau_{\text{relax}} > t_H$ . This gives a temperature of  $T_\chi^{\text{dec}} \sim 10$  MeV. Down to this temperature neutralinos on the Hubble scale belong to the radiation fluid.

Another CDM candidate is a heavy neutrino with  $m_Z/2 < m_\nu < 1$  TeV [56], where only the upper mass bound gives cosmologically relevant CDM. Again, the kinetic decoupling of these neutrinos happens way below  $T_*$ . Therefore, we find that the neutralino or a heavy neutrino would be tightly coupled to the radiation fluid during the QCD transition.

### 2. Axions

One candidate for CDM at the QCD epoch is the axion [57]. We therefore find a new mechanism to make axion clumps.

Axions could be the dominant matter today if their mass is small, i.e.  $m_a \sim 10^{-5}$  eV, which corresponds to a breaking of the Peccei-Quinn (PQ) symmetry at the scale  $f_{\text{PQ}} \sim 10^{12}$  GeV [57]. These axions could be produced coherently due to the initial misalignment of the axion field and by the decay of axionic strings. The initially misaligned axion field starts to oscillate coherently when the axion mass has grown to  $m_a(T_1) \sim 3H(T_1)$ , where  $T_1 \sim 1$  GeV [58]. Thus, below

$T_1 \sim 1$  GeV the oscillating axion field evolves as CDM,  $\rho_a \propto a^{-3}$ .

In a first-order QCD transition axionic CDM falls freely into the large potential wells from the dominant radiation fluid. This produces peaks and dips in the spectrum of axionic CDM. These peaks trigger the formation of clumps of axions with masses  $(10^{-20} - 10^{-10})M_\odot$  shortly after equality; see Sec. IV C.

Another mechanism to produce clumps of axions has been suggested in Ref. [59]. If the reheating temperature after inflation is above  $f_{\text{PQ}}$ , the axion field is inhomogeneous on scales larger than  $R_{\text{H}}(T_1)$ . Inhomogeneities in axion density evolve into axion miniclusters of typical mass  $M_{\text{mc}} \sim 10^{-12}M_\odot$  and typical radius  $R_{\text{mc}} \sim 10^8 \text{ m} \sim 0.1R_\odot \sim 10^{-3}$  AU. These axion miniclusters may be enhanced by the free-fall of matter during a first-order QCD transition. For these non-linear axion inhomogeneities a quantitative result cannot be obtained from the linear analysis of Sec. III. Let us emphasize that, in contrast to Ref. [59], we predict axion clumps independently from the reheating temperature after inflation.

### 3. Primordial black holes formed before the QCD transition

A further possibility for CDM that decoupled kinetically long before the QCD transition is primordial black holes produced before the QCD transition and therefore with masses  $M_{\text{BH}} \leq 1M_\odot$ . In order to survive until today PBHs should have  $M_{\text{BH}} > 10^{15} \text{ g} \approx 10^{-18}M_\odot$ . PBHs in the range from  $10^{-18}M_\odot$  to  $10^{-16}M_\odot$  would radiate too strongly to be compatible with  $\gamma$ -ray observations [60]. The production of PBHs arises naturally from hybrid inflationary scenarios [61,52].

Our analysis of the QCD phase transition predicts that these small black holes would be attracted by the large potential wells in the radiation fluid and would therefore tend to form miniclusters of masses up to  $10^{-10}M_\odot$ .

### C. Clumps in CDM

CDM in the form of axions or PBHs is not subject to damping as the radiation fluid; thus the peaks in CDM will survive until structure formation starts. The free streaming scale of CDM is way below our smallest scales, because the initial velocity of axions or PBHs is completely negligible. An overdensity of CDM in the form of axions or PBHs (or any other matter that is kinetically decoupled at the QCD epoch) decouples from the cosmic expansion when its density contrast becomes nonlinear,  $(\delta\rho/\rho)_R \sim 1$  (condition for turnaround). It collapses and virializes by violent gravitational relaxations and forms a clump of CDM. For spherical collapse the final viral radius is half of the radius at turnaround [62].

We take a COBE [45] normalized spectrum and allow for a tilt  $|n-1| \leq 0.2$ . During the radiation dominated regime,  $(\delta\rho/\rho)_k$  for CDM continues to grow logarithmically. In  $(\delta\rho/\rho)_R^2$  another logarithm comes from summing modes up to  $k \sim 1/R$ , where  $R$  is the radius of the window function. The enhancement factor  $\mathcal{E}$  of CDM density fluctuations during the QCD transition has been obtained in Eq. (3.55). Put-

ting these factors together we obtain the amplitude of CDM perturbations of size  $R$  at the time of equality:

$$\left(\frac{\delta\rho}{\rho}\right)_R^{\text{CDM}}(t_{\text{eq}}) \approx 2 \times 10^{-4} \left(\frac{k}{k_0}\right)^{(n-1)/2} \left[\ln\left(\frac{k}{k_{\text{eq}}}\right)\right]^{3/2} \mathcal{E}_k(t_{\text{eq}}). \quad (4.7)$$

$k_0$  denotes the comoving wave number of the mode crossing the horizon today. In the following we assume  $\Omega_0 h^2 = 1/4$ , and thus  $z_{\text{eq}} \approx 6000$ . For a CDM mass of  $10^{-15}M_\odot$  ( $10^{-20}M_\odot$ ) a tilt of  $n-1 = 0.2$  gives a factor  $\approx 16$  (23). The logarithms contribute another factor  $\approx 94$  (140). The enhancement factor has been calculated in Sec. III to be  $\mathcal{E}(t_{\text{eq}}) \approx 2$  (8) for the lattice QCD fit. Looking at  $3\sigma$  peaks we find, without tilt ( $n-1=0$ ),

$$\left(\frac{\delta\rho}{\rho}\right)_R^{3\sigma, n=1}(t_{\text{eq}}) \approx 0.1 \text{ (0.6)} \quad \text{for } M_{\text{clump}} = 10^{-15}M_\odot \text{ (} 10^{-20}M_\odot \text{)}. \quad (4.8)$$

This implies that these clumps become nonlinear at  $z_{\text{nl}} \approx 600$  (3600) and collapse to clumps of radius  $R_{\text{clump}} \approx 14R_\odot$  ( $0.04R_\odot$ ). With tilt ( $n-1=0.2$ ) we find

$$\left(\frac{\delta\rho}{\rho}\right)_R^{3\sigma, n=1.2}(t_{\text{eq}}) \approx 2 \text{ (16)} \quad \text{for } M_{\text{clump}} = 10^{-15}M_\odot \text{ (} 10^{-20}M_\odot \text{)}. \quad (4.9)$$

These overdensities start to collapse even before  $t_{\text{eq}}$  because locally CDM starts to dominate at  $\sim 2T_{\text{eq}}$  ( $16T_{\text{eq}}$ ). This leads to clump radii of  $R_{\text{clump}} \approx 0.7R_\odot$  ( $0.003R_\odot$ ).

We conclude that the peaks in the CDM spectrum lead to clumps of masses  $(10^{-20} - 10^{-10})M_\odot$ . Today, these clumps would have a density contrast of  $10^{10} - 10^{17}$ , where the lower value corresponds to a  $10^{-15}M_\odot$  clump from an untilted CDM spectrum; the bigger value is for a  $10^{-20}M_\odot$  clump from a tilted CDM spectrum. The evolution of these clumps in the late stages of structure formation remains to be investigated (disruption, mergers, etc.).

For larger enhancement, e.g., if it should turn out that the latent heat is bigger than the value from present lattice QCD calculations, more compact clumps are possible. These could be subject to femto-lensing [63]. With the values of our lattice fit, the CDM clumps are not compact enough to lie within the Einstein radius, which is  $R_{\text{E}} \sim 0.02R_\odot$  for a  $10^{-15}M_\odot$  clump.

The clumping of CDM changes the expected reaction rates for some dark matter searches, because some of the rates depend on the space-time position of the detector, star, or planet. Especially experiments looking for axion decay in strong magnetic fields [21,57] would not yield limits on the axion mass. Maybe these experiments just tell us that we are not sitting in an axion cloud currently. These consequences remain to be studied further.

## ACKNOWLEDGMENTS

We are very grateful to U. Heller and F. Karsch for providing us with their lattice QCD data sets. We like to thank J. A. Bardeen, V. Berezhinsky, B. J. Carr, U. Heller, J. Ignatius, P. Jetzer, K. Kajantie, F. Karsch, H. Markum, V. Mukhanov,

J. Silk, P. Sikivie, and N. Straumann for helpful discussions and references to the literature. C.S. thanks J. Silk and the Center for Particle Astrophysics in Berkeley for hospitality. D.J.S. and P.W. thank the Swiss National Science Foundation for financial support. D.J.S. would also like to thank the Alexander von Humboldt foundation for financial support.

- 
- [1] For recent reviews see K. Kanaya, Nucl. Phys. B (Proc. Suppl.) **47**, 144 (1996); E. Laermann, *ibid.* **63**, 141 (1998).
- [2] Y. Iwasaki *et al.*, Z. Phys. C **71**, 343 (1996); Nucl. Phys. B (Proc. Suppl.) **47**, 515 (1996).
- [3] Y. Iwasaki *et al.*, Phys. Rev. D **46**, 4657 (1992); **49**, 3540 (1994); B. Beinlich, F. Karsch, and A. Peikert, Phys. Lett. B **390**, 268 (1997).
- [4] C. Bernard *et al.*, Phys. Rev. D **54**, 4585 (1996).
- [5] J. W. Harris and B. Müller, Annu. Rev. Nucl. Part. Sci. **46**, 71 (1996).
- [6] J. Ignatius *et al.*, Phys. Rev. D **49**, 3854 (1994); **50**, 3738 (1994).
- [7] M. B. Christiansen and J. Madsen, Phys. Rev. D **53**, 5446 (1996).
- [8] E. Witten, Phys. Rev. D **30**, 272 (1984).
- [9] K. Sumiyoshi and T. Kajino, Nucl. Phys. B (Proc. Suppl.) **24**, 80 (1991); P. Bhattacharjee *et al.*, Phys. Rev. D **48**, 4630 (1993).
- [10] J. H. Applegate and C. J. Hogan, Phys. Rev. D **31**, 3037 (1985); J. H. Applegate, C. J. Hogan, and R. J. Scherrer, *ibid.* **35**, 1151 (1987); G. M. Fuller, G. J. Mathews, and C. R. Alcock, *ibid.* **37**, 1380 (1988); R. A. Malaney and G. J. Mathews, Phys. Rep. **229**, 145 (1993).
- [11] In-Saeng Suh and G. J. Mathews, Phys. Rev. D **58**, 123002 (1998).
- [12] C. Schmid, D. J. Schwarz, and P. Widerin, Phys. Rev. Lett. **78**, 791 (1997).
- [13] E. R. Harrison, Phys. Rev. D **1**, 2726 (1970); Ya. B. Zel'dovich, Mon. Not. R. Astron. Soc. **160**, 1P (1972).
- [14] V. Mukhanov and G. Chibisov, Pis'ma Zh. Éksp. Teor. Fiz. **33**, 549 (1981) [JETP Lett. **33**, 532 (1981)]; A. Starobinsky, Phys. Lett. **117B**, 175 (1982); A. Guth and S.-Y. Pi, Phys. Rev. Lett. **49**, 1110 (1982); S. Hawking, Phys. Lett. **115B**, 295 (1982).
- [15] J. M. Bardeen, P. J. Steinhardt, and M. S. Turner, Phys. Rev. D **28**, 679 (1983).
- [16] J. M. Bardeen, in *Cosmology and Particle Physics*, edited A. Zee (Gordon and Breach, New York, 1989); see also J. M. Bardeen, Phys. Rev. D **22**, 1882 (1980).
- [17] V. F. Mukhanov, H. A. Feldman, and R. H. Brandenberger, Phys. Rep. **215**, 203 (1992).
- [18] G. F. Smoot *et al.*, Astrophys. J. **396**, L1 (1992).
- [19] K. Jedamzik, Phys. Rev. D **55**, 5871 (1997).
- [20] G. Jungman, M. Kamionkowski, and K. Griest, Phys. Rep. **267**, 195 (1996).
- [21] P. Sikivie, Phys. Rev. Lett. **51**, 1415 (1983); C. Hagmann *et al.*, Phys. Rev. Lett. **80**, 2043 (1998).
- [22] MACHO Collaboration, Astrophys. J. **486**, 697 (1997); EROS Collaboration, Astron. Astrophys. **324**, L69 (1997).
- [23] P. Widerin and C. Schmid, astro-ph/9801163, 1998.
- [24] D. J. Schwarz, Mod. Phys. Lett. A **13**, 2771 (1998).
- [25] A. Chodos *et al.*, Phys. Rev. D **9**, 3471 (1974); T. De Grand *et al.*, *ibid.* **12**, 2060 (1975); T. D. Lee, *Particle Physics and Introduction to Field Theory* (Harwood Academic, Chur, Switzerland, 1981).
- [26] G. Boyd *et al.*, Phys. Rev. Lett. **75**, 4169 (1995); Nucl. Phys. **B469**, 419 (1996).
- [27] MILC Collaboration, C. Bernard *et al.*, Phys. Rev. D **55**, 6861 (1997).
- [28] J. P. Blaizot and J. Y. Ollitrault, Phys. Rev. D **36**, 916 (1987).
- [29] J. Engels *et al.*, Phys. Lett. B **396**, 210 (1996).
- [30] E. Farhi and R. L. Jaffe, Phys. Rev. D **30**, 2379 (1984).
- [31] R. Pisarski and F. Wilczek, Phys. Rev. D **29**, 338 (1984); F. Wilczek, Int. J. Mod. Phys. A **7**, 3911 (1992); K. Rajagopal and F. Wilczek, Nucl. Phys. **B399**, 395 (1993).
- [32] F. R. Brown *et al.*, Phys. Rev. Lett. **20**, 2491 (1990).
- [33] See e.g. D. H. Rischke and M. Gyulassy, Nucl. Phys. **A597**, 701 (1996).
- [34] T. DeGrand and K. Kajantie, Phys. Lett. **147B**, 273 (1984).
- [35] G. M. Fuller, G. J. Mathews, and C. R. Alcock, Phys. Rev. D **37**, 1380 (1988).
- [36] L. D. Landau, E. M. Lifschitz, and L. P. Pitajewski, *Lehrbuch der theoretischen Physik* (Akademie Verlag, Berlin, 1987), Vol. V.
- [37] L. P. Csernai and J. I. Kapusta, Phys. Rev. D **46**, 1379 (1992).
- [38] M. Hackel *et al.*, Phys. Rev. D **46**, 5648 (1992).
- [39] H. Kurki-Suonio, Nucl. Phys. **B255**, 231 (1985).
- [40] K. Kajantie and H. Kurki-Suonio, Phys. Rev. D **34**, 1719 (1986).
- [41] K. Kajantie, Phys. Lett. B **285**, 331 (1992).
- [42] M. Nagasawa and J. Yokoyama, Prog. Theor. Phys. **97**, 173 (1997).
- [43] M. Nagasawa and J. Yokoyama, astro-ph/9612014, 1997.
- [44] J. Hwang, Astrophys. J. **415**, 486 (1993).
- [45] C. L. Bennett *et al.*, Astrophys. J. **464**, L1 (1996).
- [46] A. Heckler and C. J. Hogan, Phys. Rev. D **47**, 4256 (1993).
- [47] S. Weinberg, Astrophys. J. **168**, 175 (1971).
- [48] D. L. Tubbs and D. N. Schramm, Astrophys. J. **201**, 467 (1975).
- [49] M. Crawford and D. N. Schramm, Nature (London) **298**, 538 (1982).
- [50] K. Jedamzik, astro-ph/9805147, 1998.
- [51] D. K. Nadezhin, I. D. Novikov, and A. G. Polnarev, Astron. Zh. **55**, 216 (1978) [Sov. Astron. **22**, 129 (1978)]; G. V. Bicknell and R. N. Henriksen, Astrophys. J. **232**, 670 (1979).
- [52] J. S. Bullock and J. R. Primack, Phys. Rev. D **55**, 7423 (1997).
- [53] B. J. Carr and S. W. Hawking, Mon. Not. R. Astron. Soc. **168**, 399 (1974).
- [54] C. Y. Cardall and G. M. Fuller, astro-ph/9801103, 1998.
- [55] J. Ellis *et al.*, Phys. Lett. B **413**, 355 (1997); Phys. Rev. D **58**, 095002 (1998).

- [56] J. Ellis, in *Cosmology and Large Scale Structure*, Proceedings of the Les Houches Summer School of Theoretical Physics, Les Houches, 1993, edited by R. Schaeffer *et al.* (Elsevier, Amsterdam, 1996), Session, LX, p. 825.
- [57] J. E. Kim, Phys. Rep. **150**, 1 (1987); M. S. Turner, *ibid.* **197**, 67 (1990); G. G. Raffelt, *ibid.* **198**, 1 (1990); astro-ph/9707268, 1997; P. Sikivie, hep-ph/9611339, 1996.
- [58] D. Gross, R. Pisarski, L. Yaffe, Rev. Mod. Phys. **53**, 43 (1981); M. S. Turner, Phys. Rev. D **33**, 889 (1986).
- [59] C. J. Hogan and M. J. Rees, Phys. Lett. B **205**, 228 (1988); E. Kolb and I. I. Tkachev, Phys. Rev. Lett. **71**, 3051 (1993); Phys. Rev. D **49**, 5040 (1994); Astrophys. J. **460**, L25 (1996).
- [60] B. J. Carr and J. E. Lidsey, Phys. Rev. D **48**, 543 (1993); B. J. Carr, J. Gilbert, and J. Lidsey, *ibid.* **50**, 4853 (1994).
- [61] L. Randall, M. Soljačić, and A. H. Guth, Nucl. Phys. **B472**, 377 (1996); hep-ph/9601296, 1996; J. Garcia-Bellido, A. Linde, and D. Wands, Phys. Rev. D **54**, 6040 (1996).
- [62] T. Padmanabhan, *Structure Formation in the Universe* (Cambridge University Press, Cambridge, England, 1993), Chap. 8.
- [63] A. Gould, Astrophys. J. **386**, L5 (1992); A. Ulmer and J. Goodman, *ibid.* **442**, 67 (1995).